

Tectonics

RESEARCH ARTICLE

10.1029/2019TC005523

Key Points:

- Rifting in the Eastern Black Sea Basin continued up to Oligocene, based on seismo-stratigraphic evidence for ongoing extension in the NW
- An early-Tertiary breakup was initiated in the SE part of the basin, synchronous with extension in the NW
- Sedimentary sequences record the along-strike change from synkinematic to breakup processes in the Eastern Black Sea Basin

Supporting Information:

- Supporting Information S1.

Correspondence to:

V. Monteleone,
v.monteleone@soton.ac.uk

Citation:

Monteleone, V., Minshull, T. A., & Marin-Moreno, H. (2019). Spatial and temporal evolution of rifting and continental breakup in the Eastern Black Sea Basin revealed by long-offset seismic reflection data. *Tectonics*, 38. <https://doi.org/10.1029/2019TC005523>

Received 11 FEB 2019

Accepted 6 JUN 2019

Accepted article online 17 JUN 2019

Spatial and Temporal Evolution of Rifting and Continental Breakup in the Eastern Black Sea Basin Revealed by Long-Offset Seismic Reflection Data

Vanessa Monteleone^{1,2} , Timothy A. Minshull¹ , and Hector Marin-Moreno² 

¹School of Ocean and Earth Science, University of Southampton, National Oceanography Centre Southampton, Waterfront Campus, Southampton, UK, ²National Oceanography Centre, University of Southampton Waterfront Campus, Southampton, UK

Abstract The age and distribution of the synrift and early postrift infill records the spatial and temporal distribution of extension and breakup processes in a rift basin. The Eastern Black Sea Basin (EBSB) is thought to have formed by back-arc extension during Cretaceous to Early Cenozoic time. However, a lack of direct constraints on its deep stratigraphy leaves uncertainties over the time, duration, and location for rifting and breakup processes in the basin. Here we use the enhanced imaging provided by 2-D long-offset seismic reflection profiles to analyze the deep structural and stratigraphic elements of the EBSB. Based on these elements, we infer the presence of two distinct Late Cretaceous synrift units, recording initial extension (rift stage 1) over the continental highs (Shatsky Ridge and the Mid Black Sea High), followed by strain localization along the major basin-bounding faults and rift migration toward the basin axis (rift stage 2). Overlying these units, Palaeocene(?)–Eocene and Oligocene units show a synkinematic character in the NW, with evidence for ongoing extension until Oligocene time. Toward the SE, these sequences are instead postkinematic, directly overlaying a basement emplaced during breakup. We interpret the Palaeocene(?)–Oligocene units to record the time spanning from the initiation of breakup (Late Cretaceous–Palaeocene, in the SE) to the end of extension (Oligocene, in the NW). The first ubiquitously postrift infill is the Lower Miocene Maykop Formation. Our results highlight the along-strike temporal variability of extension and breakup processes in the EBSB.

1. Introduction

Classical rifting models imply that rifting and continental breakup occur as processes well defined in time and space and recorded by distinct sedimentary sequences (e.g., Driscoll et al., 1995). However, these models are based on the interpretation of isolated transects across margins, so cannot be expected to explain the 3-D distribution of structures and sedimentary sequences along a rift system. More recently, the availability of more comprehensive data sets has allowed the documentation of the along-strike evolution at rifted margins, showing that continental rifting and breakup processes are more complex and variably distributed in time and space (e.g., Alves & Cunha, 2018; Muirhead et al., 2016; Nixon et al., 2016; Péron-Pinvidic et al., 2007; Soares et al., 2012).

In the context of intracontinental back-arc rifting, the Eastern Black Sea Basin (EBSB) is one of the most studied and yet most controversial basins in the world (Figure 1). It consists in a narrow NW trending linear trough underlain by oceanic or proto-oceanic crust, bounded by the continental domains of the Mid Black Sea High (MBSH) and the Shatsky Ridge (Figure 1a). The thickness of the sedimentary infill in the EBSB is approximately 8–9 km (Scott et al., 2009), including Cenozoic and upper Mesozoic sediments (Shillington et al., 2008). However, the deep part of the EBSB is yet to be drilled and little is known about the age and distribution of its synrift and early postrift infill. Early insights into the geological evolution of the Black Sea came from regional seismic lines (Belousov et al., 1988; Finetti et al., 1988; Tugolesov et al., 1985). Since then, researchers have attempted to unravel the kinematics, mechanisms, and timing for the opening of the EBSB (e.g., Finetti et al., 1988; Görür, 1988; Graham et al., 2013; Nikishin et al., 2003; Okay et al., 1994; Rangin et al., 2002; Robinson et al., 1996; Shillington et al., 2008; Stephenson & Schellart, 2010). In addition, crustal-scale industry seismic data sets have been acquired due to the growing interest in the EBSB as a region with high hydrocarbon potential, related to the presence of a regionally

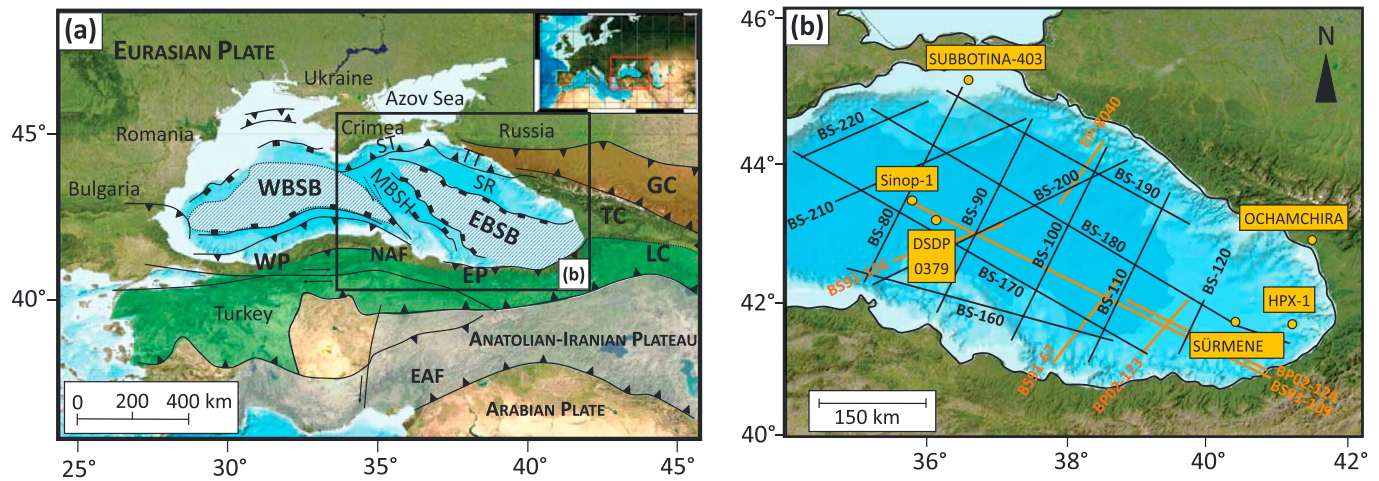


Figure 1. (a) Topographic and structural map of the Black Sea and Caucasus region (www.emodnet-bathymetry.eu). The black box represents the study area (b). Structural elements highlighted are EBSB/WBSB, Eastern/Western Black Sea Basins; SR, Shatsky Ridge; MBSH, Mid Black Sea High; TT/ST, Tuapse/Sorokin Troughs; GC/LC, Greater/Lesser Caucasus; TC, Transcaucasus; EP/WP, Eastern/Western Pontides; NAF/EAF, North/East Anatolian Fault. (b) Bathymetry and topography map of the EBSB. The black lines mark the long-offset seismic reflection profiles. The orange lines mark other profiles used. The yellow dots mark deep-water and onshore wells in the area. Sürmene-1, Sinop-1, HPX-1, and Subbotina-403 well locations are from Kitchka et al. (2014), Sydorenko et al. (2017), and Tari and Simmons (2018). The location for the onshore well Ochamchira is from Banks et al. (1997).

distributed source-rock, the Maykop Formation (e.g., Graham et al., 2013; Robinson et al., 1996; Stovba et al., 2009).

The identification of synrift stratigraphic intervals is essential to understand the evolution of rifted margins, as they record the early stages processes in a rift system. However, the determination of these synrift sequences is often complicated by a lack of data and of direct constraints (e.g., Péron-Pinvidic et al., 2007). In the EBSB, wells penetrating the entire Cenozoic and part of the Mesozoic sections are located along the margins or onshore, while strata of this age lie at depths ≥ 8 km in the center of the basin. Therefore, stratigraphic sections at well locations are comparatively condensed, and there are uncertainties in tracing major horizons from well locations into the basin center (Shillington et al., 2008). Also, most of the wells have been drilled in the Western Black Sea Basin (WBSB), and tracing horizons from the WBSB to the EBSB is challenging because of the presence of the MBSH, which prevents direct correlation of horizons older than Late Eocene (Banks et al., 1997).

Seismic data have also been used to define the presence and distribution of the synrift in the EBSB, but imaging is often limited by attenuation through the thick basin infill (e.g., Finetti et al., 1988; Rangin et al., 2002; Shillington et al., 2008). In fact, in most studies, synrift geometries (e.g., fanning reflector geometry toward fault planes) are not clearly observed in seismic data (e.g., Nikishin et al., 2015a; Shillington et al., 2008). Therefore, synrift units may be mistaken for prerift or postrift strata because of the lack of obvious growth beds (Withjack et al., 2002). This ambiguity may explain the small thickness of synrift deposits identified in the EBSB (e.g., Görür et al., 1993; Görür & Tüysüz, 1997).

Here we interpret and discuss the deep seismo-stratigraphic framework of the EBSB using long-offset seismic reflection profiles acquired in 2011 by Geology Without Limits (GWL) and ION GXT, which provide enhanced imaging at depth, combined with published litho-stratigraphy and well-correlated seismic data. Isopach maps, seismic facies, and examples of seismic profiles are presented to illustrate the characteristics, areal distribution, and thickness of each unit. The aim of this study is to present the distribution and ages of the synrift, early postrift, and postrift sequences, to analyze their stratigraphic contacts and their interaction with the structural features of the basin. These elements are used to define rift onset, propagation, and breakup stages in the EBSB.

Unraveling the rifting and breakup processes controlling EBSB formation has a key role in understanding the geodynamic evolution of this area and of similar rift systems. Furthermore, this study provides fundamental insights into (i) how deformation is accommodated in space and time and (ii) how

stratigraphic and structural elements track strain distribution and localization during the process of continental extension.

2. Geological Framework

2.1. Geological Evolution of the EBSB Region

The EBSB is a deep sedimentary basin lying between the Eastern Pontides and the Great Caucasus mountain ranges (Figure 1a). Rifting is the first-order geodynamic process responsible for the tectonic evolution of the EBSB and is related to the northward subduction of the Neotethys Ocean below the Eurasian Plate (Finetti et al., 1988; Görür, 1988; Nikishin et al., 2003; Okay et al., 1994; Robinson et al., 1996; Stephenson & Schellart, 2010; Zonenshain & Le Pichon, 1986). The basin opened in a back-arc setting behind the Pontides magmatic arc (Finetti et al., 1988; Görür, 1988; Okay et al., 1994; Zonenshain & Le Pichon, 1986). Back-arc extension was generated by the counter-clockwise rotation of the Shatsky Ridge away from the MBSH, as evidenced by paleo-magnetic data (Westphal et al., 1986). Compressional forces and tectonic inversion, due to the northward movement of the Arabian Plate, started along the Pontides in the Late Cretaceous, reaching the Greater Caucasus possibly in the Palaeocene and becoming regionally widespread during the Late Eocene and Oligocene (Espurt et al., 2014; Hippolyte et al., 2017; Munteanu et al., 2011; Robinson et al., 1996; Vincent et al., 2016). The syncollisional (orogenic) stage is generally considered to have started in the Oligocene, forming the Caucasus mountain range and causing the uplift of some areas within tectonic units as well as the reactivation of older fault systems and the formation of inverted structures (Stovba et al., 2009). Compressive deformation is concentrated around the edges of the EBSB, as shown by seismic reflection data, earthquake locations, and subsidence analysis (e.g., Edwards et al., 2009; Shillington et al., 2008).

2.2. Available Data on the Basin Stratigraphy

Detailed analyses of the thicknesses and distribution of the sedimentary deposits in the EBSB are based on the most updated interpretation of seismic data (e.g., Kazmin et al., 2000; Nikishin et al., 2003, Nikishin, Okay, et al., 2015a; Scott et al., 2009; Sydorenko et al., 2017), and estimates on the age and lithology of the sedimentary units generally come from seismic stratigraphic horizons tied to well control at the edges of the basin and to onshore outcrops (e.g., Greater and Lesser Caucasus, and Crimean Mountains; Nikishin et al., 2003, Nikishin et al., 2015a, Nikishin et al., 2015b; Okay et al., 2013; Robinson et al., 1996; Saintot et al., 2006; Stephenson & Schellart, 2010; Stovba et al., 2009). More reliable information comes from dredged sequences from the Archangelsky Ridge (Rudat & MacGregor, 1993) and from a complete Mesozoic to Lower Palaeocene stratigraphy in wells drilled over the Shatsky Rise in Georgia (Robinson et al., 1996). These stratigraphic interpretations have fed into paleo-geographic reconstructions of the mechanisms and timing of basin opening (e.g., Egan & Meredith, 2007; Nikishin et al., 2015b; Okay et al., 1994; Robinson et al., 1996; Stephenson & Schellart, 2010).

Extensive deepwater drilling has occurred in the WBSB, whereas only four deep wells have been drilled in the EBSB to date (e.g., Stovba et al., 2009; Sydorenko et al., 2017; Tari & Simmons, 2018; Figure 1b). Subbotina-403 reaches 4,300 m below seabed and terminates in the Lower Eocene succession (Stovba et al., 2009; Sydorenko et al., 2017; Figure 1b). Sinop-1, 5,531 m deep, was drilled on a structural high of Andrusov Ridge, targeting a synrift of Aptian to Albian age (e.g., Tari & Simmons, 2018; Figure 1b). The sediment cover above the MBSH and the Shatsky Ridge has been described by using extensive academic and industry seismic reflection data (e.g., Belousov et al., 1988; Nikishin 2015a, 2015b; Rangin et al., 2002; Robinson et al., 1996; Tari et al., 2018), crustal scale wide-angle seismic data (e.g., Shillington et al., 2017; Yegorova et al., 2010), and seafloor dredging (Rudat & MacGregor, 1993). Chronostratigraphic charts have been compiled to illustrate the different ages and litho-stratigraphy elements of the Black Sea region and EBSB (Adamia et al., 2017; Shillington et al., 2008; Sydorenko et al., 2017; Tari & Simmons, 2018).

Figure 2 and Table 1 summarize previous attempts to estimate the timing of rifting in the EBSB. Note that the definition of rift duration changes from author to author: it can be either the time from rift initiation to breakup (e.g., Nikishin et al., 2015a) or the time from rift initiation to the end of oceanic spreading (e.g., Okay et al., 1994). Some studies assume that the EBSB opened at the same time as the WBSB, and provide age estimates, which are mostly based on data coming from the WBSB region (e.g., Hsü et al., 1977; Tüysüz, 1999). Based on different data, rifting has been considered to be Jurassic (e.g., Zonenshain &

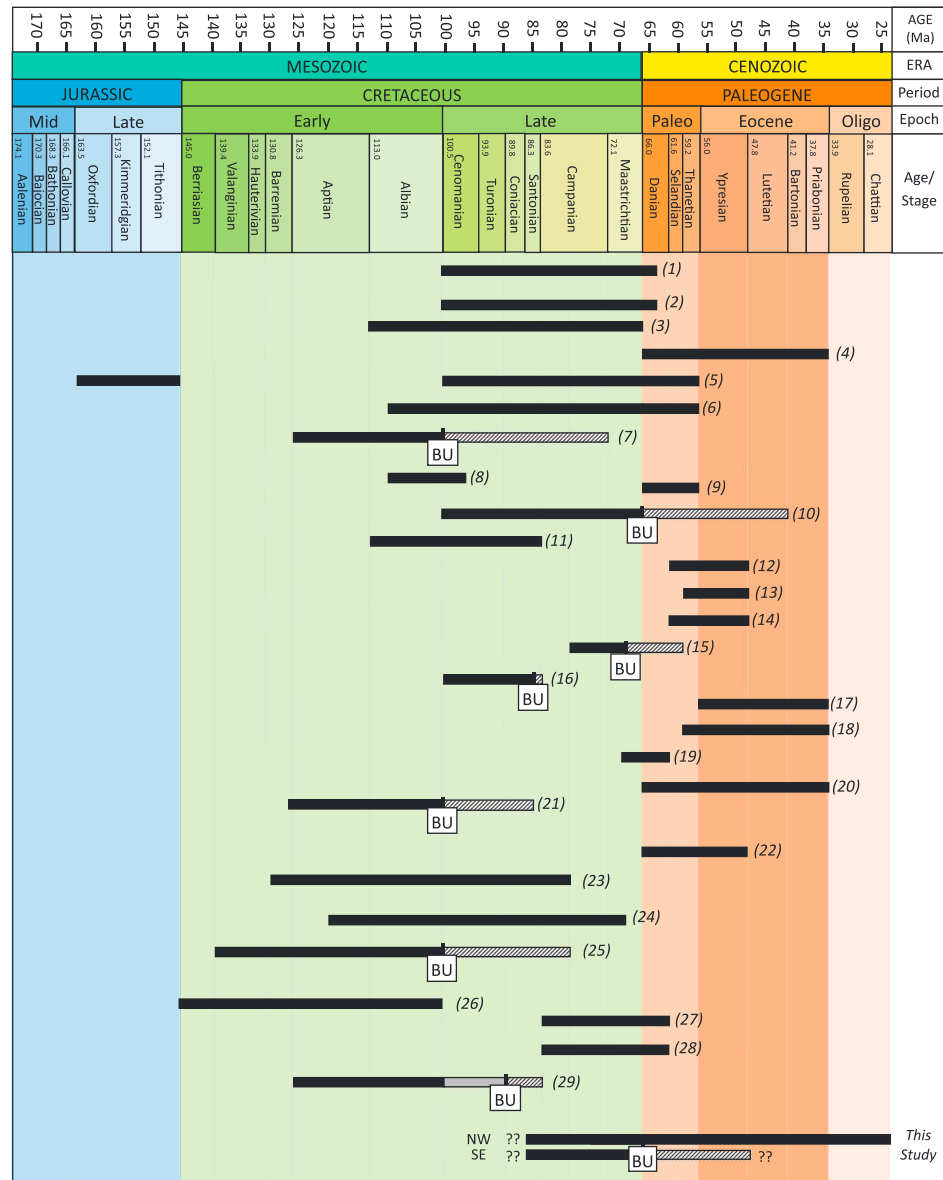


Figure 2. Timing of rift and breakup in the Eastern Black Sea Basin from previous studies. The black bar indicates rift duration. The grey bar indicates the age of a second synrift deposit identified by Tari and Simmons (2018). When available, timing of breakup (BU) and oceanic spreading are shown (hashed bar). Numbers correspond to the studies listed in Table 1. The geological time-scale is adapted from Cohen et al. (2016).

Le Pichon, 1986), Cretaceous (e.g., Adamia et al., 1974; Görür, 1988; Nikishin et al., 2003; Okay et al., 1994), Early Cretaceous to Palaeocene (e.g., Finetti et al., 1988; Sydorenko et al., 2017), Palaeocene to Early Eocene (e.g., Banks et al., 1997; Robinson, Spadini, et al., 1995), or Eocene (e.g., Kazmin et al., 2000; Yilmaz et al., 2000) in age. From the analysis of the Crimean Mountains onshore outcrops, and from micropaleontological dating (nanno-plankton) in the same region, studies infer similar timing for the EBSB rift (starting in Early Cretaceous), breakup (Albian-Cenomanian), and oceanic spreading (Cenomanian to Santonian/Campanian; e.g., Hippolyte et al., 2018; Nikishin et al., 2003; Sheremet et al., 2016). Conversely, studies based on Georgia and Eastern Pontides onshore outcrops generally infer a Late Cretaceous-Early Cenozoic basin opening (e.g., Okay et al., 1994; Yilmaz et al., 2000). Similarly, studies integrating wells data from the Shatsky Ridge and dredging from the Archangelsky Ridge infer a Palaeocene-Eocene age for rifting (e.g., Banks et al., 1997; Rudat & MacGregor, 1993; Spadini et al., 1996). Depending

Table 1

Table Listing in Chronological Order the Studies Used as a Reference for the Previous Estimated Time of Rifting and Breakup in the EBSB

#	List of authors	Data used to constrain timing of rift
(1)	Adamia et al. (1974)	Structural relationships from EBSB coastline, ages of magmatism, and plate reconstruction
(2)	Letouzey et al. (1977)	Geological observations and seismic reflection data analysis
(3)	Hsü et al. (1977)	Plate reconstruction
(4)	Tugolesov et al. (1985)	Seismic data interpretation
(5)	Zonenshain and Le Pichon (1986)	Seismic evidences and subsidence history analysis
(6)	Finetti et al. (1988)	Seismic reflection data and onshore observations
(7)	Görür (1988); Görür and Tüysüz (1997); Görür et al. (1993)	Paleogeography based on geological observations and stratigraphy Central Pontides
(8)	Golmshtok et al. (1992)	Seafloor heat-flow measurements and multichannel data
(9)	Rudat and MacGregor (1993)	Wells data from Shatsky Ridge in Georgia and dredging from Archangelsky Ridge
(10)	Okay et al. (1994); Okay and Şahintürk (1997); Okay and Tüysüz (1999)	Structural/stratigraphic evidences and age of magmatic products of Eastern Pontides
(11)	Bektaş and Güven (1995)	Age of magmatism in Eastern Pontides
(12)	Robinson, Banks, et al. (1995), Robinson, Spadini, et al. (1995), Robinson et al. (1996)	Seismo-stratigraphic interpretation and well data
(13)	Spadini et al. (1996)	Kinematic modeling and thermal structure analysis
(14)	Banks et al. (1997)	Onshore outcrops, well data, and seismic interpretation onshore Georgia
(15)	Shreider et al. (1997); Shreider (2005)	Magnetic anomaly studies
(16)	Tüysüz (1999); Tüysüz et al. (2012)	Analysis of volcanogenic rocks in north Turkey
(17)	Yilmaz et al. (2000)	Structural correlations (Transcaucasus and Eastern Pontides), and age of magmatism
(18)	Kazmin et al. (2000)	Thickness and distribution of Palaeocene-Eocene sedimentary units from seismic data
(19)	Verzhbitsky et al. (2002)	Heat-flow analysis and seismic data interpretation
(20)	Cloetingh et al. (2003)	Thermo-mechanical modeling
(21)	Nikishin et al. (2003, 2011, 2013, 2015b), Nikishin, Wannier, et al. (2015)	Correlation of Crimean onshore geology and regional seismic reflection profiles
(22)	Shillington et al. (2008)	Integration of onshore geological mapping, well data and seismic reflection data
(23)	Stovba et al. (2009)	Seismic data interpretation and correlation with Subbotina-403, -1 wells
(24)	Stephenson and Schellart (2010)	Geo-dynamic modeling of back-arc extension
(25)	Hippolyte et al. (2010, 2017, 2018)	Structural and stratigraphic analysis in Crimes and Pontides, and nannoplankton ages
(26)	Sheremet et al. (2016)	Micro-paleontological dating sampled on the Crimean Mountains
(27)	Vincent et al. (2016)	Subsidence analysis.
(28)	Sydorenko et al. (2017)	Seismic interpretation offshore Crimea and correlation with Subbotina-403 well
(29)	Tari (2015); Tari and Simmons (2018)	Stratigraphic compilation of published information and well data

Note. Numbers in the left column refer to the time bar shown in Figure 2. For each of the studies, the methodology used to determine the time-constraints is briefly described.

on the location of the sampling, there are different outcomes in terms of timing for rifting and breakup in the EBSB.

3. Data and Methods

3.1. Seismic Data

We used 12 poststack time-migrated long-offset seismic reflection profiles, acquired in 2011 by GWL and ION GXT (Figure 1b). Seismic profiles were acquired using an air gun array with total volume of 5,680 cu. in., 816 channels, a 10,200-m-long streamer, and an 18-second (two-way travel time) record length. Processing was carried out by GWL and consisted in editing, low-cut filtering, spherical divergence correction, multiple suppression (predictive deconvolution and radon de-multiple), amplitude balancing, normal

moveout correction, muting and stacking, poststack Kirchhoff time migration and poststack/postmigration band-pass filtering, coherent filtering, and amplitude balancing. Long-offset profiles are integrated with six time-migrated multichannel seismic reflection profiles, acquired by BP before 2005 (Figure 1b). These profiles were acquired with streamer lengths of 3,600 to 6,000 m, allowing 8 to 15-second (two-way travel time) record length, and they were used to constrain the shallower seismo-stratigraphic interpretation. We converted the time migrated profiles to depth using interval velocities derived from the stacking velocities provided by GWL, combined with velocities from wide-angle seismic data (Shillington et al., 2009, 2017). A comparison between the GWL velocities and those from wide-angle seismic profiles, which have a sufficiently large aperture to constrain the velocities of deep sediments, showed that the two velocity functions are very similar in the shallow section (above basement reflection), while wide-angle seismic velocities are faster in the deeper section. In order to provide the most accurate velocity model for time-depth conversion, we combined these two velocity fields. Further information on the time-depth conversion steps is given in the supporting information.

3.2. Seismic Interpretation: Method and Terminology

Regionally distributed prominent reflectors, characterized by discordant stratigraphic contacts and variations in seismic character, extend across the EBSB. These reflectors were used to identify the top and base of separate sedimentary sequences (S1-S7). We used the internal geometries and seismic facies variation of these sequences (Figures 3–7), as well as their interaction with structural elements across the basin, to identify their prerift, synrift, or postrift character (e.g., Franke, 2013; Williams, 1993). Seismic horizons interpreted in depth were gridded using a Convergent Interpolation algorithm (e.g., Haecker, 1992) and a cell size of 250×250 m to generate horizon structural surfaces. Thickness maps for each sedimentary sequence (isopach maps) were calculated from the difference between the horizon surfaces representing top and base of that sequence. Isopach maps are presented to illustrate the depocenter distribution and their spatial and temporal migration (Figure 8).

Normal fault systems were mapped and interpolated across seismic profiles, where possible. The resulting fault polygons were overlain on isopach maps to help to define fault-related depocenter development (Figure 8). Fault planes have been picked from discontinuities in reflections, from residual diffractions and from sedimentary infill geometries.

In this paper we classify the identified unconformities based on the stratigraphic models of Bond et al. (1995), Falvey (1974), and Franke (2013), which recognize two key unconformities that develop during rifting and continental breakup: the *rift-onset unconformity*, which separates prerift and synrift strata, and the *breakup unconformity*, which separates synrift from postrift strata at the time of crustal breakup and onset of oceanic crust accretion (e.g., Falvey, 1974; Withjack et al., 1998). The *breakup unconformity* is defined as an erosional surface characterizing the uplifted margins during rifting stage, often truncating wedge-shaped synrift sediments and separating them from younger postrift sequences that show little/no evidence of extension controlling their deposition (Franke, 2013). Basinward, this unconformity merges with an angular unconformity and terminates onto the top of the igneous crust (Franke, 2013). However, a clear definition of this unconformity as a single stratigraphic surface, together with the identification of distinct synrift and postrift stratigraphic sequences, is complicated by the fact that rifting and continental breakup processes are variably distributed in time and space (e.g., Péron-Pinvidic et al., 2007). In this study we define the presence of a *breakup unconformity* of regional extent, which is the principal stratigraphic feature related to continental breakup along the continental highs. Downslope and in the central basin this unconformity becomes a stratigraphic contact between distinct sedimentary sequences and/or the contact between the top of the inferred oceanic crust and the overlying sequence. Due to the complex definition of rift and breakup processes, previous studies introduced the idea of a *transition sequence* recording the gradual transition from synrift to postrift stage (e.g., Moore, 1992). This idea has been further developed by more recent studies, acknowledging breakup as a prolonged event identified by a discernible unconformity-bounded stratigraphic sequence of regional extent, showing distinct depositional architectures compared to older (synrift) strata and younger (postrift) units: the *breakup sequence* (e.g., Alves & Cunha, 2018; Soares et al., 2012). Here we refer to a recent definition of *breakup sequence* by Soares et al. (2012), which describes the character of some sedimentary units deposited from the onset of lithospheric breakup to the establishment of thermal relaxation as the main process controlling the subsidence of the basin.


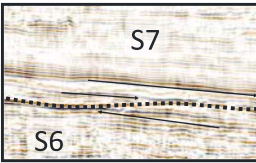
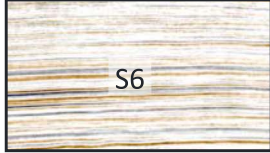
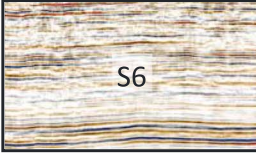
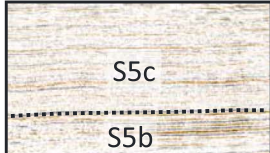
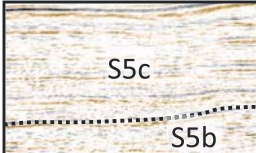
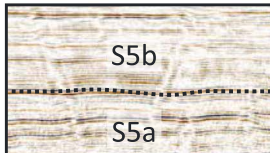

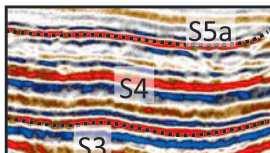
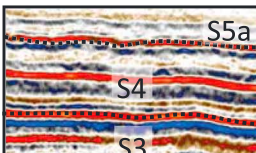
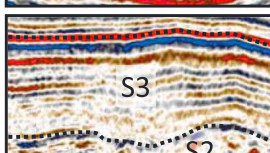
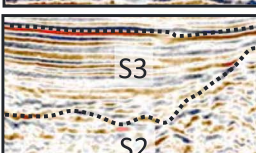
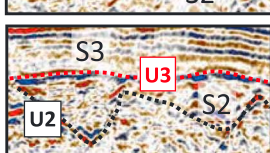
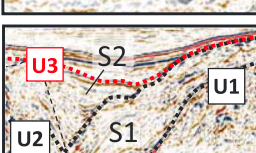
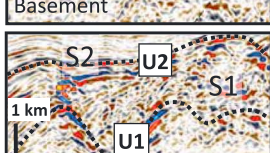
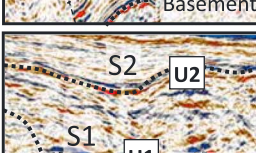
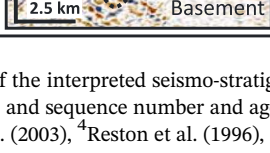
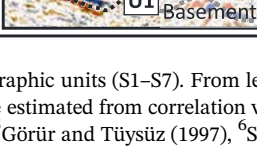
SEISMIC FACIES		LITHO-STRATIGRAPHY	SEQ #
		<ul style="list-style-type: none"> ◆ Plio-Quaternary sediments. ◆ Mostly clays, including marls and occasional turbidites¹. 	<p>S7 (11-1.8 Ma)</p>
		<ul style="list-style-type: none"> ◆ Upper Miocene interval². ◆ The shallower sequence (13-11 Ma) comprises terrigenous sediments³. 	<p>S6 (20.5-11 Ma)</p>
		<ul style="list-style-type: none"> ◆ Oligocene-Early Miocene Maykop Formation. ◆ Hydrocarbon source rock in the Black Sea and Caspian Sea. ◆ Muds rich in organic carbon with very little sand⁴. 	<p>S5 (33.9-20.5 Ma)</p>
			
			
		<ul style="list-style-type: none"> ◆ S3 and S4 associated to Palaeocene(?)–Lower Eocene and Middle–Upper Eocene formations, respectively. ◆ Eocene succession is composed by dominantly silicoclastic turbidites (sandstones and shales)^{5–6}. 	<p>S4 (45-33.9 Ma)</p>
			<p>S3 (45-65? Ma)</p>
		<ul style="list-style-type: none"> ◆ The basement consists of Upper Jurassic to Cretaceous (over the MBSH) or Upper Cretaceous (over the Shatsky Ridge) limestones. ◆ The overlain sequences (S1–S2) are associated to the Upper Cretaceous interval⁷. 	<p>S2 (65?–? Ma)</p>
			<p>S1</p>

Figure 3. Summary of the interpreted seismo-stratigraphic units (S1–S7). From left to right: seismic examples for each sequence, litho-stratigraphy information from previous studies, and sequence number and age estimated from correlation with previous studies. References: ¹Ross (1978), ²Robinson, Banks, et al. (1995), ³Nikishin et al. (2003), ⁴Reston et al. (1996), ⁵Görür and Tüysüz (1997), ⁶Sydorenko et al. (2017), and ⁷Robinson, Spadini, et al. (1995).

4. Seismic Data Analysis

4.1. Structural Elements

The main rift-related structural elements of the EBSB are illustrated in profile bs-90 (Figure 4a). To the NE, the Shatsky Ridge is a basement high bounded to the south by one or more large normal faults (Shatsky Ridge fault), with a northern flank that is flexed beneath the Greater Caucasus, generating a small foreland basin, the Tuapse Trough (Figure 4a). On the western and south-western side of the basin are the

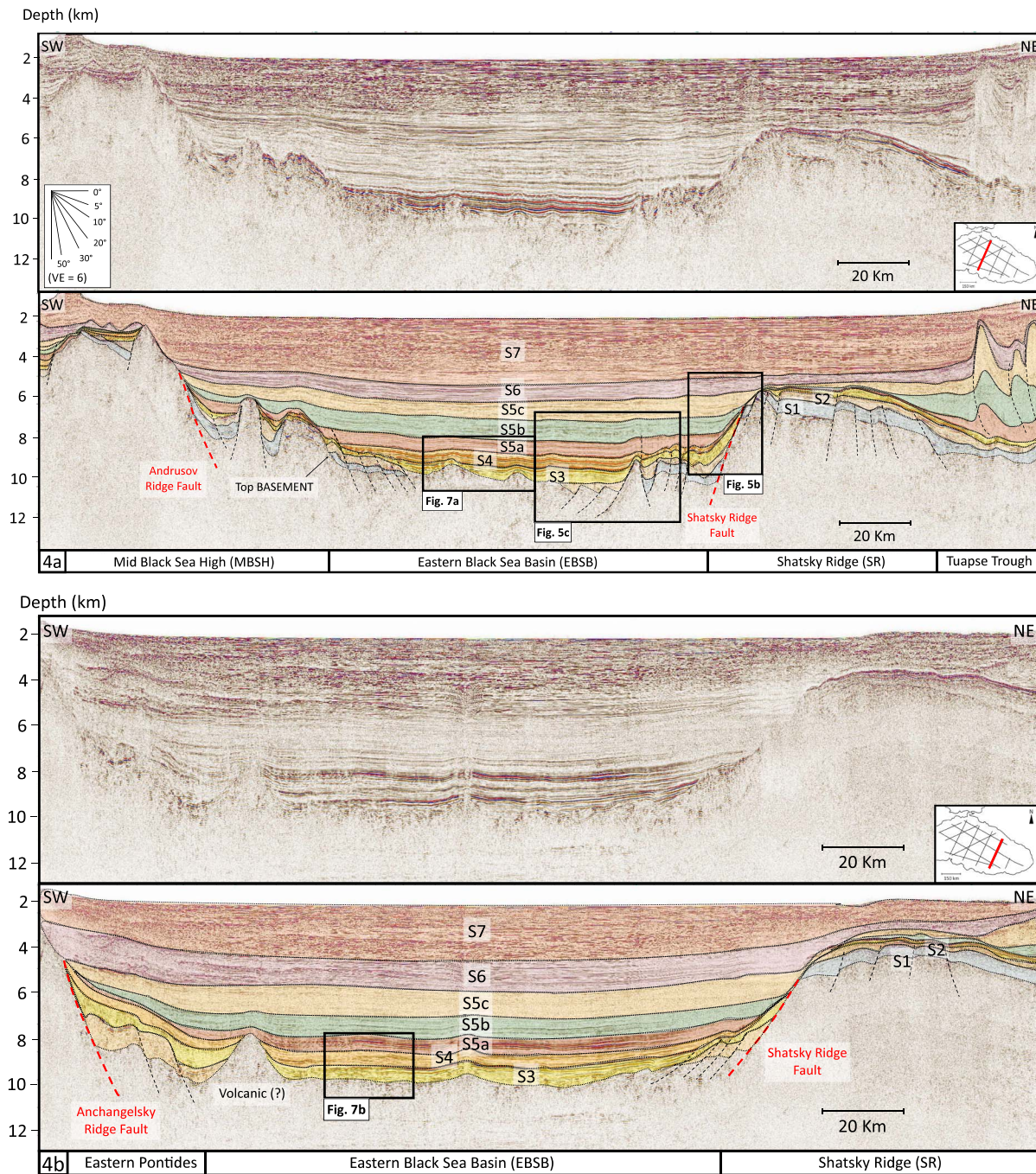


Figure 4. (a) Profile bs-90. The MBSH and the Shatsky Ridge bound the central EBSB. Colors mark interpreted stratigraphic sequences (S1 to S7). The top basement is affected by normal faults (dashed lines) generating tilted crustal blocks. Normal faults over the structural highs generally show higher dip angle (30° - 70°), whereas downslope they show lower dip angle (15° - 25°). Synkinematic deformation is mainly visible within units S1 and S2, but it affects also shallower units S3-S4 and S5a, at locations. The main fault planes are interpreted in continuity across NE-SW trending profiles (red dotted lines): Shatsky Ridge fault and Andrusov Ridge fault. The black boxes show the locations of Figures 5b, 5c, and 7a. (b) Profile bs-110. A major change in the character of the deep sedimentary infill is visible: no clear synkinematic deformation affects sequences S3 and S4, which have instead a clear postrift character, directly overlying the central EBSB basement. The Shatsky Ridge fault is mapped across from profile bs-90, showing here a lower dip angle. The Andrusov Ridge fault is also mapped across nearby profiles. A volcanic body has been interpreted at the SW end of this profile by previous studies (e.g., Nikishin et al., 2015a). The black box shows the location of Figure 7b. (VE = 6:1).

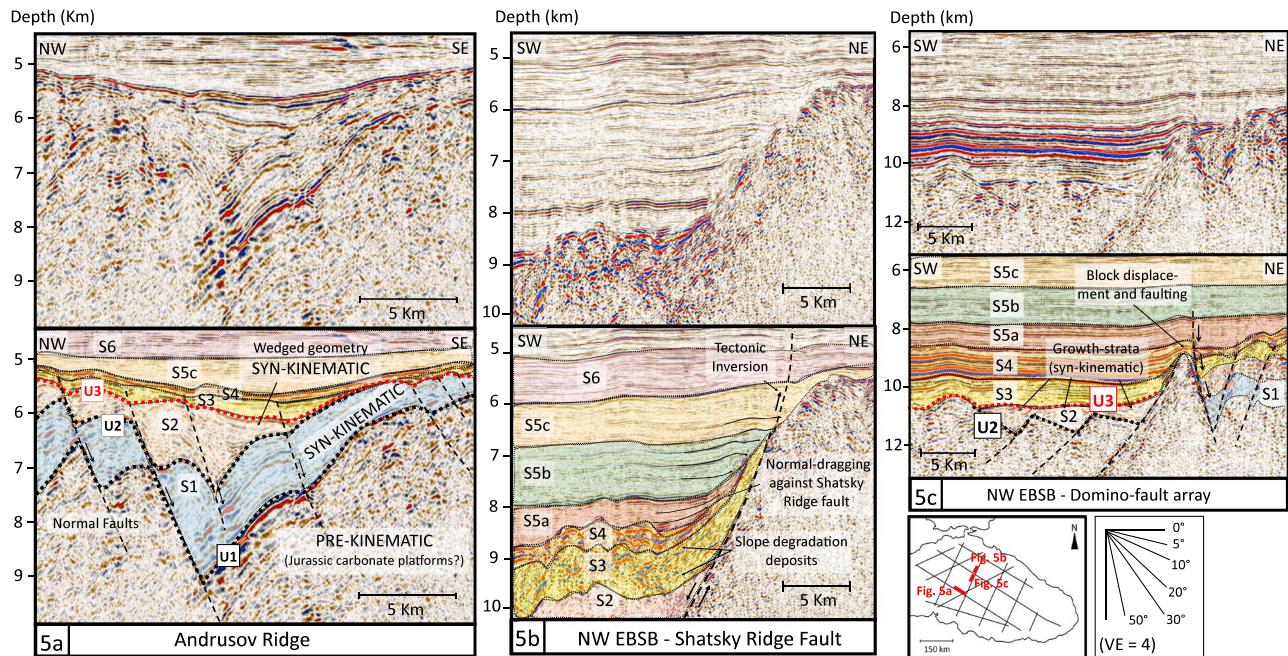


Figure 5. (a) Part of profile bs-170, showing synrift wedged geometries (S1-S2). The contact between S1 and the basement is defined by unconformity U1. S2 overlies S1 in angular discordance, defining unconformity U2. Horizon U3 identifies the top of S2 and the base of sequence S3. Sequences S3 and S4 are a thinner sedimentary cover over the structural highs. (b) Part of profile bs-90. The Oligocene Maykop Formation (S5a) shows strata dragging along the Shatsky Ridge fault. The Miocene Maykop Formation (S5b-S5c) pinches-up over the same fault plane, indicating compressive reactivation along this fault. S3 and S4 units resemble the character of chaotic slope degradation deposits (VE = 4:1). (c) Part of profile bs-90. Downslope, wedged S2 deposits represent the main synrift infill, overlying tilted fault-blocks. S1 is generally absent. The base of the well layered S3 unit truncates the S2 wedges, defining unconformity U3. (VE = 3:1).

Archangelsky and Andrusov Ridges (MBSH). Various evidence for extensional tectonics is visible, with normal faults generally showing a NW-SE to WNW-ESE trending direction and bounding graben and half-graben structures (Figures 4a, 4b, 5a-5c, 6a, 6b, and 8). Basinward, normal fault arrays are organized in closely spaced domino faults (Figure 5c). All the identified faults cut the basement (prerift) and the deep sedimentary sequences (S1 and S2). The main fault systems, interpolated across the seismic profiles,

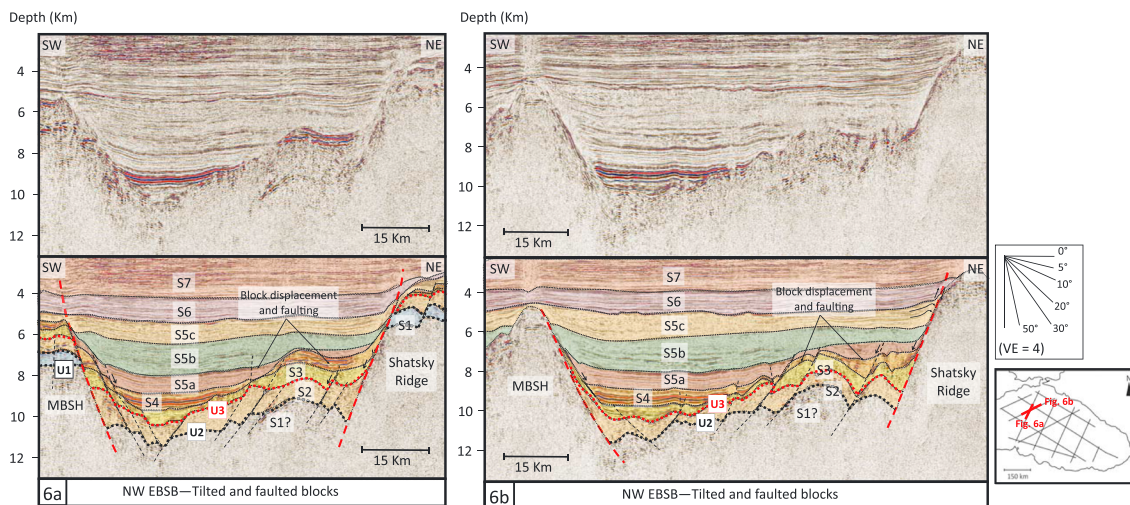


Figure 6. Profiles showing fault activity through S3, S4, and S5a units: (a) part of profile bs-80; (b) part of profile bs-210. In both examples, faulting and tilting of continental blocks occur up to the Oligocene Maykop Formation (S5a). The resulting synkinematic topography is then progressively smoothed out by the Miocene Maykop Formation (S5b and S5c). The red dashed lines are the Shatsky Ridge fault (NE) and the Andrusov Ridge fault (SW). Mapped unconformities U1, U2, and U3 are also shown. Evidence for S5c pinching-up over the Shatsky Ridge fault (b) indicates compressive reactivation along this fault (see also Figure 5b). (VE = 4:1).

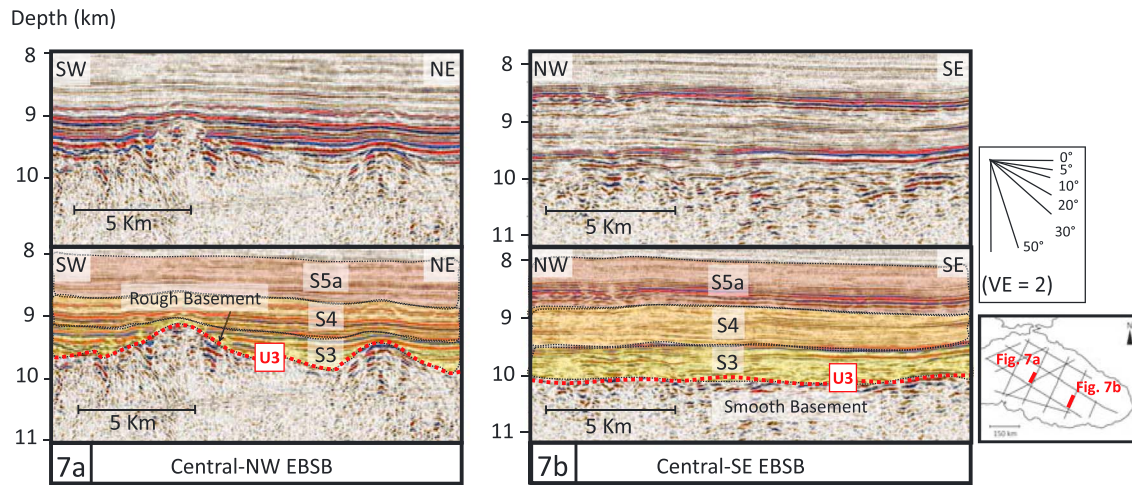


Figure 7. (a) Part of profile bs-90 (location in Figure 4a). There is no evidence for synrift deposits in this area. S3 directly overlies the top of a rough basement, the morphology of which affects S3 thickness distribution (Figure 8c). (b) Part of profile bs-110 (location in Figure 4b). No evidence for synrift deposits in this area. S3 directly overlies a smooth basement, which is considered to have formed due to breakup and spreading in this area.

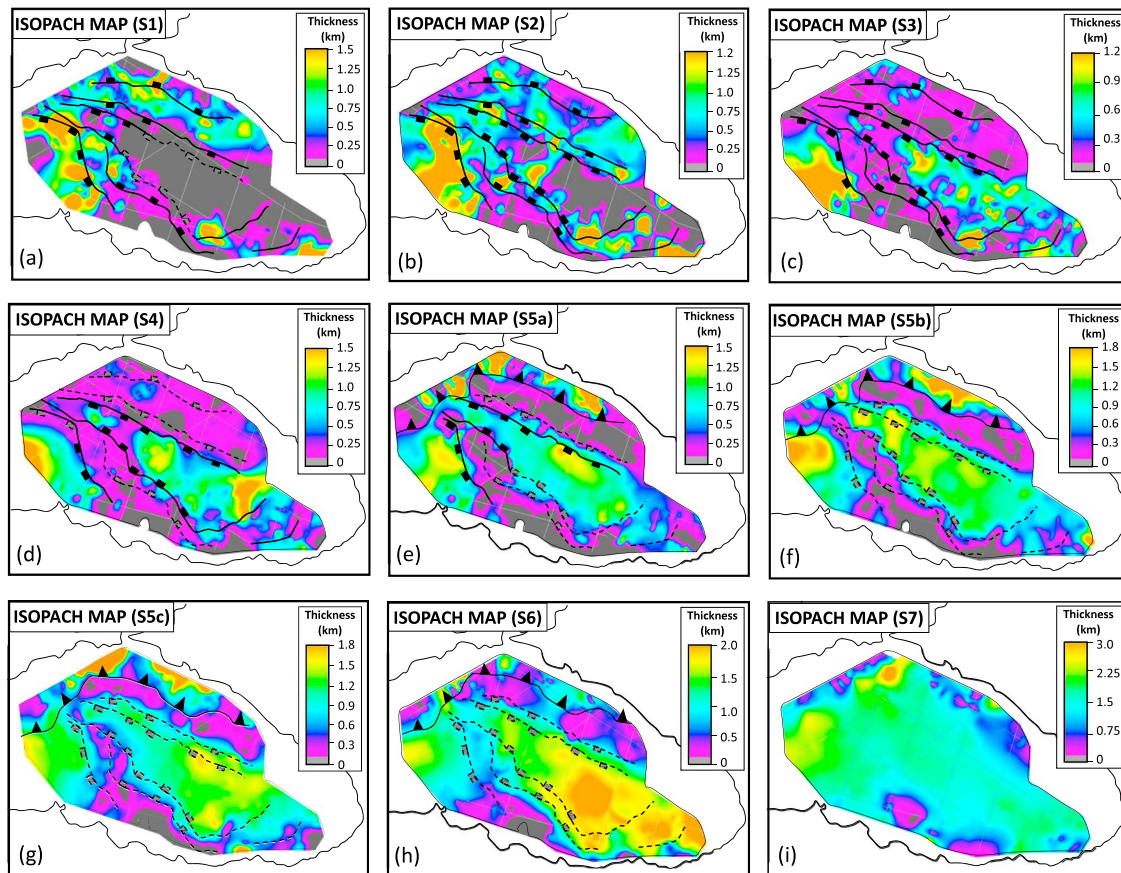


Figure 8. Isopach maps. (a) S1—visible over the structural highs and rapidly thinning basinward (Rift stage 1); (b) S2—visible basinward (NW), records strain migration toward the basin axis (Rift stage 2); (c) S3—Palaeocene(?)–Early Eocene sequence, progressively infilling the central EBSB; (d) S4—Middle–Upper Eocene; (e) S5a—Oligocene Maykop Formation. S3, S4, and S5a record ongoing extension in the NW, and a localized breakup in the SE; (f) S5b—Lower Miocene Formation, showing the end of extension and the beginning of a regionally spread postrift subsidence; (g) S5c—Middle Miocene Maykop Formation. Thickness changes along basin-bounding faults are linked to compressional reactivation; (h) S6—Top Miocene, showing a greater amount of sediment supply in the SE, and (i) S7—Pliocene–Quaternary, progressively filling the all basin. Fault systems have been tentatively interpreted with a continuous black line (the fault was active during the time represented by that sequence), or with a dashed line (ceased/not started fault activity at that time).

are the basin-bounding faults also representing the flanks of Shatsky Ridge and MBSH (Figures 4a, 4b, and 8). The sedimentary sequences immediately overlying faulted basement blocks allow us to estimate the age and duration of fault activity. The faults affecting the basement highs generally show a variable but mostly high dip angle (30-70°; Figure 5a), whereas basinward faults arrays have quite a uniform and low dip angle (15-25°; Figure 5c). The velocity model used for seismic depth conversion affects the dip angle of the interpreted faults. Below basement, time-depth conversion using wide-angle velocities results in faults with dip angles up to 4-5° steeper than those from using stacking velocities. This difference in fault dip angle is similar to the 1-2° dip angle uncertainty from the standard deviation in wide-angle velocities (see the supporting information). Another change from the structural highs to the central basin is represented by the different stratigraphic contacts with the top of the faulted basement blocks. Over the ridges, S1 is the dominant infill, while S2 is the prevalent infill within basinward half-graben structures (Figures 4a, 5a, 5c, 6a, and 6b). In the central and SE parts of the basin, there is no evidence for normal faults (Figures 4a and 4b). The top basement is a corrugated surface becoming progressively smoother to the SE (Figures 7a and 7b). In this area, faults affecting the basement generate basement scarps that have been described in previous studies as the result of interpreted ENE-WS trending trans-tensional faulting (Shillington et al., 2009).

4.2. Seismo-stratigraphic Elements

We mapped the acoustic basement and seven sedimentary sequences across the EBSB, based on their seismic facies, internal geometries, and interaction with structural elements (Figure 3). Some of the deepest and thus oldest, fault-bounded sequences are discontinuous throughout the basin. This lack of continuity, together with the presence of gaps between seismic profiles, prevents a clear correlation of these sequences at a regional scale. This point has to be considered when looking at isopachs for these sequences (especially S1 and S2), particularly in areas where seismic coverage is low. With this point in mind, we describe the interpreted sequences below, starting from the oldest, S1 (deepest), and moving to the youngest, S7 (shallowest):

S1 is a low-amplitude seismic unit with isolated higher-amplitude reflections (Figure 3). Despite the general lack of coherency of its seismic facies, it can be present as a well-layered infill of graben and half-graben structure (Figures 3, 4a, and 5a). The S1 isopach map shows that S1 is present over the tops of the MBSH and the Shatsky Ridge, where it is 250 to 1,500 m thick (Figure 8a). It then rapidly thins downslope to disappear toward the central basin (Figures 4a, 4b, and 5c). S1 is bounded by two unconformities (horizons U1 and U2), marking the discordant contact at its base and top with the underlying basement and the overlying S2 sequence. Horizon U1 is, in some places, a very high reflectivity boundary (Figure 5a). In contrast, horizon U2 is a low-amplitude reflection (Figure 5a). S1 is a tectonically controlled sedimentary infill, with strata thickness changes and wedged geometries bounded by normal fault planes (Figures 4a and 5a).

S2 is a medium- to low-amplitude sequence, showing layered packages organized into sedimentary wedges bounded by normal faults (Figures 3, 4a, 5a, and 5c). Along the main basin-bounding faults, S2 is sometimes a chaotic and semitransparent package resembling a detrital material deposited downslope and subsequently overlapped by chaotic to well-layered younger sedimentary sequences (S3-S4; Figures 4a, 5b, 6a, and 6b). S2 is up to ~1,500 m thick and is often confined within small depocenters (Figure 8b). S2 occurs as secondary infill above S1, on the top of Shatsky Ridge and the MBSH, while it is a primary infill of basinward half-graben structures (Figures 4a and 5c). Within these half-graben structures, S1 may be still present below S2, although not properly imaged. The top of S2 is defined by unconformity U3 (Figures 4a, 4b, 5a, 5c, 6a, and 6b). The progressive basinward thinning of S1 and S2 causes the related unconformities U1 and U2 to merge in the basin center, and here only the top U2 horizon is interpreted (Figure 5c). Further basinward thinning of S2 causes the coalescence of horizons U2 with U3, leaving horizon U3 as the contact between S3 and the top basement (Figures 5c, 7a, and 7b). The S2 isopach map shows the uneven distribution of this unit through the basin (Figure 8b). Compared to S1, which is mostly interpreted over the Shatsky Ridge, the MBSH, and the Tuapse and Sorokin Troughs, S2 exists further basinward, in the NW (Figure 8b). In the SE, S2 is interpreted along the basin-bounding faults, but it is absent in the central basin (Figures 4b and 8b).

S3 is generally a well-layered sequence, with low-amplitude reflections at its base and higher amplitudes toward its top (Figure 3). In the NW, down the Shatsky Ridge slope, this sequence has the character of a chaotic detrital deposit (Figures 5b, 6a, and 6b). Seismic profiles and isopach map show that this unit is preferentially distributed in the central basin (with maximum thickness up to 1,200 m), while it is <500 m thick over the MBSH and the Shatsky Ridge (Figure 8c). Thickness changes are partly a response to the underlying

basement topography (Figures 4a and 7a), affecting the distribution of S3 in the central basin, but also a response to tectonic activity visible in the NW part of the basin and along the main basin-bounding faults (Figures 4a, 5c, 6a, and 6b). In these areas normal faults crosscut S3, indicating a synkinematic deposition (Figures 5c, 6a, and 6b).

S4 is characterized by subparallel, high- to low-amplitude reflections (Figure 3). The top and base of this sequence are identified by high acoustic impedance contrasts with the base of S5a (lower Maykop Formation) and the top of S3, respectively (Figure 3). Tectonic control is less visible within this sequence, but some normal faults propagate through S4 generating small thickness changes (Figures 5c, 6a, and 6b). S4 is deposited mainly in the central basin (500 to 1,250 m thick), while it is a drape of sedimentary cover over the continental highs (≤ 250 m thick; Figure 8d). S4 is generally more uniformly distributed in the central basin compared with the older sequence S3.

S5a, S5b, and S5c units are associated to the regionally distributed Maykop Formation characterized by a semitransparent seismic layer (e.g., Robinson et al., 1996; Sydorenko et al., 2017; Zonenshain & Le Pichon, 1986). S5 is indeed a low-amplitude package with homogeneous appearance, generally linked to uniformity in its lithological character. This sequence is up to $\sim 4,500$ m thick in the central basin, thinning over Shatsky Ridge and the MBSH (≤ 500 m thick), and thickening again along the compressed margins of the EBSB (Tuapse and Sorokin Troughs), where it can reach thicknesses of 2,500 to $\geq 5,000$ m (Figures 8e, 8f, and 8g). Although the Maykop Formation is usually interpreted as a single sedimentary package, we subdivide it into three layers: S5a, S5b, and S5c (Figures 3, 4a, 4b, 5b, 6a, and 6b). This subdivision is marked by the presence of weak but laterally continuous reflectors, probably linked to lithological variation within the unit. Within the lower Maykop Formation (S5a) some high reflectivity layers are probably related to the intercalation of more sandy interbeds (e.g., Stovba et al., 2009). Extensional faults propagate through S5a sequence generating small thickness changes (Figures 5c, 6a, and 6b). Furthermore, the lateral termination of S5a on the Shatsky Ridge fault shows evidence of normal-drag (the hanging wall beds dip away from the normal fault; Withjack et al., 2002) along the fault plane (Figures 5b and 6b). In contrast, S5b and S5c show no particular evidence for extensional tectonics, and their strata onlap in reverse-drag (the hanging wall beds dip toward the normal fault; Withjack et al., 2002) onto the basin-bounding faults (Figures 5b and 6b). S5a, S5b, and S5c isopach maps show depocenter migration through time (Figures 8e, 8f, and 8g). S5a has quite a uniform distribution in the central basin, with visible thickness changes controlled by normal fault activity along the Shatsky Ridge fault, and thrust fault activity along the NE margin of the EBSB (Figure 8e). The compressional tectonics is associated with the folding and thrusting visible in the seismic data, also affecting the shallower units S5b and S5c (Figures 4a and 5b). The S5b main depocenter is located in the NW corner of the basin (Figure 8f), whereas S5c main depocenter migrates toward the SE (Figure 8g). No clear tectonic control is visible within these units, so depocenter migration is probably due to a change in the main source of sediment supply. Furthermore, small thickness changes along fault planes, visible in the S5b and S5c isopach maps, may be related to the compressive reactivation of the basin-bounding faults (Figures 5b, 6b, and 8g).

S6 and S7 are well-layered and subparallel, medium to high reflectivity units with alternating semitransparent strata (Figure 3). They represent the shallowest and youngest sequences filling the basin. Our interpretation matches previous seismic interpretation and well data correlation (e.g., Nikishin et al., 2015a; Shillington et al., 2008). The thickness of sequence S6 is up to 2,500 m in the central basin, while sequence S7 reaches a thickness of 100-2,000 m across the EBSB (Figures 8h and 8i). S6 is thicker toward the SE part of the basin, perhaps related to the main source of sediment supply in that area (Figure 8h).

5. Discussion

5.1. Character and Distribution of the EBSB Sedimentary Infill

5.1.1. Age of the Interpreted Sequences

There are no new well data available for this study, so we rely on published information to define the age and litho-stratigraphy of the interpreted sequences. The Palaeocene(?)–Eocene to recent EBSB infill is generally well known and considered as a postrift, based on onshore and offshore drilling (e.g., Ross, 1978; Sydorenko et al., 2017), whereas the age and distribution of the synrift sequences is much less constrained. Synrift units

interpreted on seismic data rely mostly on onshore observations (e.g., in Turkey, Crimea and Georgia). However, correlation of the synrift laying in the central basin with its approximate onshore equivalent requires the assumption that the timing of rifting is synchronous across this region.

The age of the interpreted sequences S1 and S2 is difficult to constrain, for the reasons stated above. Sequences overlying S2 are instead within depths investigated by some of the offshore drilling, especially in areas where those sequences have been uplifted by Eocene compression (e.g., Hippolyte et al., 2018; Sydorenko et al., 2017). In the N-NE part of the EBSB, offshore Crimea, the Subbotina-403 and -1 wells reached the Neogene and Oligocene-Eocene sequence (Stovba et al., 2009; Tari & Simmons, 2018). The oldest sequence identified consists in sediments of Lower Eocene age. Above them, lies the Oligocene-Miocene Maykop Formation (corresponding to S5 units). Seismic data from the northern EBSB, correlated to Subbotina-403 well, are presented by Stovba et al. (2009) and Sydorenko et al. (2017). These profiles cross some of our seismic lines (bs220, bs180, bs210, and bs80), so we can correlate our interpreted sequences with this well stratigraphy. Sydorenko et al. (2017) interpreted a single sequence beneath the Maykop Formation, which includes the Palaeocene-Eocene deposits and corresponds to our S3-S4 units. Below that sequence, they interpreted an undifferentiated Cretaceous sequence, probably including our S1 and S2 units, which overlies an Upper Jurassic prerift in the northern part of the Shatsky Ridge.

Comparing the stratigraphic information from Subbotina-403 with the seismic facies of our interpreted sequences, we further subdivide the Palaeocene-Eocene unit. The S3 medium to low reflectivity facies, with high reflectivity toward the top (Figure 3), corresponds to the Lower Eocene sequence litho-stratigraphy sampled by Subbotina-403, which is made of marls interlayered with clay and sandy layers toward the top (Sydorenko et al., 2017). The seismic character of sequence S4 (Figure 3) matches well with the Middle-Upper Eocene sequences sampled by Subbotina-403, showing alternating shale and sandy units, with sandy layers dominating top and base of the sequence, which would generate strong acoustic-impedance contrasts. Based on this evidence, we define S3 to be Palaeocene(?)–Lower Eocene (45–65 Ma) unit and S4 Middle-Upper Eocene (45–33.9 Ma) unit. Consequently, the underlying sequences S1 and S2 represent an undifferentiated Upper Cretaceous infill, in agreement with other studies (e.g., Shillington et al., 2008; Sydorenko et al., 2017; Tari & Simmons, 2018).

From published litho-stratigraphy it is possible to define sequences S5a, S5b, and S5c as the Oligocene and Lower-Middle Miocene part of the Maykop Formation, while S6 and S7 correspond to the Upper Miocene and Plio-Quaternary, respectively (e.g., Hippolyte et al., 2018; Sydorenko et al., 2017). Here we subdivide the Maykop Formation into three sequences (S5a–S5b–S5c). This subdivision is due to the presence of regional, medium-low reflectivity horizons that we interpret as the top and base of further packages into which this sequence is subdivided (Figures 3, 4a, 4b, 6a, and 6b). The presence of these reflective boundaries within the Maykop Formation may be related to a change in the sedimentary character and physical properties of the sequence. The Maykop Formation is considered to be an overpressured layer (e.g., Scott et al., 2009), so this subdivision may imply a compartmentalization of the overpressure within the sequence. A previous subdivision of the Maykop Formation is described by Jones and Simmons (1997). This layering within the Maykop Formation is not only representative for the potential variability in its physical and lithological properties, but it also associates to a different synkinematic (S5a) to postkinematic (S5b–S5c) character of the sequence.

5.1.2. Rift Stage

Although some studies have interpreted the presence of a synrift infill in the EBSB (e.g., Shillington et al., 2008; Sydorenko et al., 2017; Tari & Simmons, 2018), most authors tend to agree on the absence/near absence of synrift deposits in the central EBSB (e.g., Görür et al., 1993; Görür & Tüysüz, 1997), due to the lack of strong evidence for synrift sedimentary geometries on seismic profiles (e.g., Nikishin et al., 2015a).

In our seismic profiles, syntectonic growth structures and wedge geometries bounded by normal faults are clear features over the Shatsky Ridge and the MBSH (Figures 4a and 5a). Here, overlying a faulted prerift (basement), sequences S1 and S2 (Upper Cretaceous) are interpreted as two distinct synrift deposits with a combined thickness up to 3 km (Figures 4a, 5a, 5c, 8a, and 8b). Studies based on onshore observations also identified the presence of two synrift sequences in the region (e.g., Hippolyte et al., 2018; Nikishin et al., 2015a; Tari & Simmons, 2018). We define the contact between prekinematic (basement) and S1 as

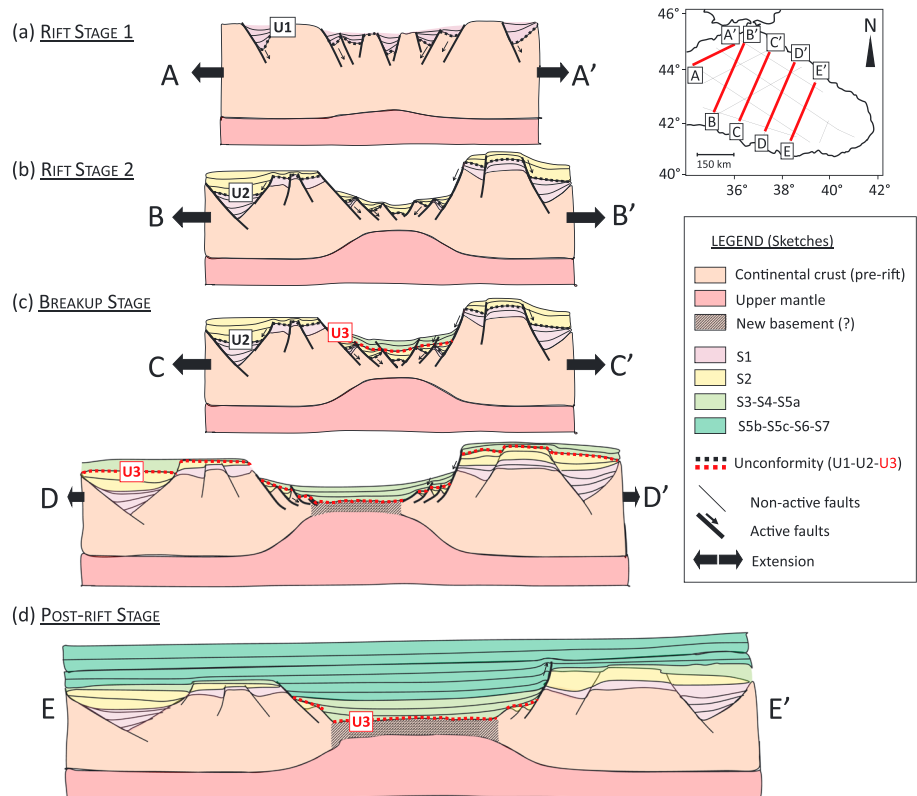


Figure 9. A summary of the Eastern Black Sea Basin evolution, with sketches based on seismic reflection profiles from different parts of the basin (sketches not in scale). (a) Rift Stage 1: Crustal stretching (low β) forming isolated depocenters (*Rift Onset Unconformity* - U1), bounded by high-angle normal faults (30°-70° dip). Graben and half-grabens are filled by synrift (S1) (b) Rift Stage 2: Isolated faults coalesce forming main basin-bounding faults and extension migrates toward the basin axis, where increased crustal thinning (high β) is accommodated by lower angle (15°-25° dip) fault arrays. Half-grabens are filled by the younger synrift (S2). Unconformity U2 records the basinward migration of rifting. (c) Breakup Stage: Its onset is marked by unconformity U3. Units S3, S4, and S5a show extension up to Oligocene time (S5a) in the NW, synchronous to localized breakup and spreading in the SE, where these units show a clear postrift character (d). (d) Postrift Stage: The Lower Miocene Maykop Formation represents the first widespread postrift infill. Sketch profile locations are plotted over the survey map on the top right corner.

unconformity U1, which we interpret as a *rift-onset unconformity* (Franke, 2013; Withjack et al., 2002), marking the initial rifting event affecting the structural highs (Rift stage 1, Figure 9a). This unconformity progressively merges basinward with the stratigraphically younger unconformity U2 (base of S2 unit) forming a composite unconformity (Figures 4a, 5a, and 5c). The merging of these unconformities is due to the gradual thinning of S1 toward the basin center, where half-graben structures are mostly filled by the younger synrift (S2) instead (Figures 4a, 5a, and 5c). The presence of an unconformity like U2, separating the early synrift strata from the later synrift strata, is a common feature in other rift basins (e.g., Buckley et al., 2015; Lei et al., 2019; Olsen, 1997). This unconformity shows the basinward migration of extension in the EBSB, associated with a progressive younging of the synrift infill toward the rift axis (Rift stage 2 - Figure 9b). This two-stage rifting is visible in S1 and S2 isopach maps, where there is a clear basinward propagation of the main depocenter location (Figures 8a and 8b).

Rift migration is also recorded by a change in the character and age of the extensional faulting. Faults interpreted over the structural highs generally show higher dip angles (30°-70°). Here the faulted basement is covered by the older S1 unit, and fault activity continues through the S1 and S2 units, stopping at the base of S3 unit (Figures 4a and 5a). Downslope, faults are organized into more closely spaced domino-fault arrays, characterized by lower dip angles (15°-25°; Figures 4a and 5c). In this area, the faulted basement is directly overlain by the younger synrift sequence (S2), and faults propagate sometimes into shallower units (up to S5a) steepening upward (Figures 5c, 6a, and 6b). Fault initiation and duration can be constrained by the

age of the synkinematic infill, so basinward faults formed later than those interpreted over the ridges. Similar evidence for synkinematic units recording the formation of faults that young oceanward is observed along other rift basins and rifted margins (e.g., Nixon et al., 2016; Péron-Pinvidic et al., 2007; Ranero & Pérez-Gussinyé, 2010; Reston, 2005). Various observational studies and numerical models show that rifting starts within a network of isolated normal fault segments generating a moderate crustal thinning (low β) and distributing deformation across the area (e.g., Cowie et al., 2000; Nagel & Buck, 2004; Péron-Pinvidic et al., 2017). As stretching continues, some faults grow laterally and coalesce into dominant basin-bounding single faults (e.g., Cowie et al., 2000). Deformation focuses along these few active, larger faults, whereas smaller faults along the less thinned rift flanks become inactive (e.g., Cowie et al., 2000; Ranero & Pérez-Gussinyé, 2010). As strain progressively migrates and focuses toward the future basin center, sequentially active normal faults form to accomplish rift migration (e.g., Brune et al., 2014; Nagel & Buck, 2004; Ranero & Pérez-Gussinyé, 2010). During this stage, further crustal thinning (high β) and increasing accommodation space occurs. In the EBSB, we consider high angle normal faults to record the initial stage of distributed faulting (Figure 9a), followed by subsequent fault linkage and generation of the master faults bounding the structural highs (Figure 9b). Continued extension then causes the border faults to experience more strain and basinward focusing of crustal thinning accompanied by the generation of new, lower angle sequential faults accommodating the basinward propagation of stretching (Figures 9b and 9c). The seaward decrease in fault dips is predicted by the rolling hinge model of Buck (1988) and Lavier et al. (1999). Evidence for normal faults initiating at higher dip angles and then rotating to lower angles during progressive extension is visible at other rifted margins (e.g., Ranero & Pérez-Gussinyé, 2010; Reston, 2005), and back-arc basins (e.g., Lei & Ren, 2016). This model may explain the progressive change in fault dip observed in the EBSB. Based on both stratigraphic and structural elements in the EBSB, we recognize a two-stage rifting process, initiating by widespread extension (Figure 9a) and followed by rift migration and strain focusing toward the basin axis (Figure 9b). Our observations from the EBSB are similar to those from other rift basins and rifted margins such as the Bay of Biscay (e.g., Tugend et al., 2015), the Iberia-Newfoundland margin (e.g., Brune et al., 2017; Ranero & Pérez-Gussinyé, 2010; Reston, 2005), the Brazil-Angola margin (e.g., Brune et al., 2017), the Gulf of Corinth (e.g., Nixon et al., 2016), and the northern margin of the South China Sea (e.g., Lei et al., 2019; Lei & Ren, 2016).

5.1.3. Breakup Stage

In our seismic interpretation, S3 lies in angular unconformity over the tilted and faulted blocks, covering the S1-S2 wedged geometries on the structural highs and crosscutting, basinward, the tops of the S2 wedges (Figures 5a and 5c). The angular contact between S3 (Palaeocene(?)-Eocene) and S2 (Upper Cretaceous) defines unconformity U3 (Figures 5a and 5c). Based on the geometrical relationship of the contact between S2 and S3, U3 can be interpreted as a *breakup unconformity* (Falvey, 1974; Franke, 2013). Basinward, U3 becomes instead the stratigraphic contact between S3 and the underlying basement (Figures 4b, 7a, and 7b). Previous studies interpreted the Palaeocene(?)-Eocene units as a postrift infill (e.g., Nikishin et al., 2015a; Sydorenko et al., 2017). However, there is evidence for normal fault propagation within these units in the NW part of the basin (Figures 5c, 6a, and 6b), together with evidence for strata terminations dragged upward along the main basin-bounding fault planes, indicating extensional activity during their deposition (Figures 5b and 6b). Similarly, S5a (Oligocene Maykop Formation) shows evidence for active extension in the NW (Figures 5c, 6a, and 6b). Isopach maps highlight the irregularity of the S3 and S4 infills (Figures 8c and 8d). These irregularities partly result from the topography of the underlying basement affecting the distribution of the infill (Figure 7a) and/or may be related to differential compaction processes. However, observations along NW seismic profiles show clear evidence for active faulting during S3-S4 deposition (Figures 5c, 6a, and 6b). The S5a sequence appears to be more uniformly distributed across the basin, but fault activity observed along NW seismic profiles (Figures 5c, 6a, and 6b), together with thickening toward the Shatsky Ridge fault visible on the isopach map, suggests fault activity during the time of S5a deposition (Figure 8e).

Moving toward the central and SE part of the basin, there is no clear evidence of active extension in the S3 to S5a units. Here, these sequences appear like a typical postrift infill overlying a basement reflection (Figures 4b, 7a, and 7b). The crustal velocity structure, determined from ocean bottom seismometer data, suggests that the SE part of the EBSB is underlain by thick oceanic crust (Shillington et al., 2009). This interpretation agrees with the lack of evidence for extension, and with the postrift character of S3-S5a sequences

in this part of the basin. Therefore, S3-S5a probably consists of marine sediments deposited during and after the breakup and spreading in the SE of the basin. The S3-S4-S5a units show an along-strike change in stratigraphic character that appears to be intermediate between synrift and postrift sequences. The seismic character of these units shows similarities with the definition of *breakup sequences* given by Soares et al. (2012) and Alves and Cunha (2018). Similar to this definition, S3 to S5a units record the transitional period between the onset of breakup (SE) and the end of extension (NW), followed by the establishment of thermal relaxation as the main process controlling subsidence in the basin. Based on seismic evidence along the west Iberia-Newfoundland margins, Alves and Cunha (2018) identified within the *breakup sequence* distinct seismic intervals of chaotic to partly continuous seismic reflections terminating against the slope fault system and interpreted these intervals as mass-wasting and turbiditic deposits associated to the breakup stage. These units are then gradually draped by wavy to subparallel, low-amplitude seismic reflections interpreted to reflect the spreading conditions on a fully developed margin. Similarly, we recognize that S3 and S4 units are locally organized in chaotic deposits linked to slope degradation processes, overlain by the younger and semitransparent units of the Maykop Formation (Figures 5b, 6a, and 6b). This may be seen as a further evidence of the comparable character between our S3, S4, and S5a units and the *breakup sequence* defined by Soares et al. (2012), both recording the diachronous evolution of breakup processes at extensional settings. Based on these considerations, and on similarities with observations coming from other studies (e.g., Péron-Pinvidic & Manatschal, 2009; Soares et al., 2012), S3 to S5a units are interpreted to record a diachronous breakup stage across the EBSB (Figure 9c).

These considerations imply that the defined *breakup unconformity* (U3) cannot be considered representative of a widespread end of rifting and breakup initiation across the EBSB, as we need to acknowledge the temporal and spatial variability of these processes across the basin (e.g., Péron-Pinvidic et al., 2007). The breakup stage (Figure 9c) is therefore time constrained by the ages of S3 to S5a infills, which show that extension continued up to Oligocene time in the NW, whereas breakup started before the deposition of S3 (Palaeocene(?)-Early Eocene time) in the SE, synchronous with the NW ongoing extension. The total thickness of S3 to S5a sequences ranges from 1.8 to 4-4.5 km in the central basin. Because these units form part of the synkinematic infill in areas where extension was active up to Oligocene time, they are considered to contribute to the overall thickness of the synrift deposits of the EBSB.

5.1.4. Postrift Stage

Seismic data show no evidence for extensional tectonics within S5b, S5c, S6, and S7 units (Figures 6a and 6b). As these sequences all show a ubiquitous postrift character, we consider the onset of thermal relaxation to be represented by the Lower Miocene Maykop Formation (S5b; postrift stage; Figure 9d). Isopach maps show that these postrift sequences progressively infill the preexisting topography, while compression starts deforming the sediments accumulated along the NE margin (Tuapse and Sorokin Troughs; Figures 8f, 8g, and 8h). Thickness changes within these sequences are associated with depocenter migration related to a change in the source of sediment supply through time, probably partially controlled by compressional deformation along the peripheral regions of the basin.

5.2. Final Considerations

The identification of synrift stratigraphic intervals is a very important aspect in the study of rifted margins (e.g., Péron-Pinvidic et al., 2007). In the EBSB, we defined the presence of two clear synrift units (S1 and S2), which are ascribed to two separate Late Cretaceous extensional stages (Figures 9a and 9b). S3 to S5a units (Palaeocene(?) to Oligocene) are also interpreted to represent part of the synkinematic infill along the NW part of the basin, where active tectonics affects their deposition (Figures 6a and 6b). Previous studies suggested various timings for the synrift and thus for the basin opening, such as Aptian-Albian (e.g., Görür, 1988; Hippolyte et al., 2018), Cenomanian-Turonian-mid Santonian (e.g., Tari & Simmons, 2018; Tüysüz, 1999), or Palaeocene-Early Eocene or Eocene (e.g., Banks et al., 1997; Kazmin et al., 2000; Robinson, Banks, et al., 1995; Robinson, Spadini, et al., 1995), based on onshore data and well data acquired at different locations across the EBSB region. Similarly, breakup process has been estimated to be either Albian-Cenomanian (e.g., Görür, 1988; Hippolyte et al., 2018; Nikishin et al., 2015b), Turonian-Coniacian (e.g., Tari & Simmons, 2018), mid-Santonian (e.g., Tüysüz, 1999), or Maastrichtian-Danian (e.g., Okay et al., 1994, 2013; Shreider, 2005). Our study highlights the variable distribution of rifting and breakup processes at different locations and times in the basin. This distribution is recorded within the variable architecture

and stratigraphic character of the identified sequences, showing either a synkinematic or postkinematic character. With this observation in mind, the definition of rifting and breakup ages would be strictly dependent on the location of the study, and not really representative of the timing of the process on a regional scale. This complexity may explain such a variety of results and the general disagreement between different studies.

The EBSB is a multistage narrow rift formed by initial widespread stretching (Figure 9a), followed by rift migration toward the basin axis (Figure 9b), and progressive strain localization into the area of the future breakup (Figure 9c). Once breakup and spreading initiated along the more extended SE segment, extension continued along the less extended NW segment. This is well expressed by the Palaeocene(?)–Eocene and Oligocene sequences, which have both a synkinematic character in the area where extension continued up to Oligocene (NW; Figure 9c), and a postkinematic character in the area where breakup and “new” basement was generated (SE; Figure 9d). Together with the along-axis variability in sedimentary ages and architecture, the change in character of the extensional faulting records the different rifting stages (e.g., Lavier & Manatschal, 2006; Moore, 1992; Péron-Pinvidic et al., 2007; Sutra et al., 2013). Starting as isolated high angle normal faults, some of these systems merged to form the main basin-bounding faults. Strain then migrated toward the basin axis forming younger, low-angle domino-fault arrays, associated with the progressive localization of rifting into the area of the future breakup (Figures 9a–9c). This along-strike variability in fault geometry and sedimentary architecture reflects a specific kinematics of basin opening. Several studies have proposed models to explain formation and evolution of V-shaped basins (e.g., Le Pourhiet et al., 2018; Lundin et al., 2014; Nirrengarten et al., 2018; Taylor et al., 1995; Zhou et al., 1995). Some models refer to a “scissor-like” opening (e.g., Hey et al., 1980), whereas other invoke a rift propagation or “zipper-slider” opening style, where the tip point of extension initiates in one area to then “jump” (e.g., Taylor et al., 1995) or progressively migrate along with further rift propagation (e.g., Martin, 1984; Vink, 1982). The analysis of oceanic crust magnetic isochrons provides key information for the identification of propagation mechanisms, as it may reveal the diachronous development of oceanic crust younging toward the pole of rotation, thus allowing the reconstruction of its evolutionary pattern (e.g., Franke, 2013; Lundin et al., 2014). The three-dimensional modeling of Le Pourhiet et al. (2018) simulates various scenarios for the opening mechanism of the V-shaped South China Sea basin, showing that a “scissor-like” model contradicts evidence from magnetic isochrons and conjugate margin structure, whereas previous studies invoked such a mechanism for this back-arc opening (e.g., Zhou et al., 1995). Recent studies have investigated the Southern North Atlantic basins to understand the partitioning and propagation of deformation, proposing a modified version to the model of oceanic propagation (e.g., Martin, 1984) by introducing the idea of segmented propagation controlled by the presence of transform faults (Nirrengarten et al., 2018).

Our observations of along-strike variations in temporal and spatial patterns of extension show clear evidence for rift propagation, associated with progressive basin opening. Although it is generally assumed that the EBSB opened around a “fixed” rotation pole located in Crimea (e.g., Okay et al., 1994), thus implying a “scissor-like” opening kinematic, sediment distribution, and fault patterns seem to indicate that the tip of the propagator could have migrated in time from SE to NW. To test this idea, detailed three-dimensional mapping of the fault distribution and of the deep sedimentary sequences is required in order to date the migration of deformation across the basin (e.g., Péron-Pinvidic et al., 2007). The sparse coverage of our data set in some areas precludes such mapping. A lack of clear seafloor spreading anomalies over the inferred oceanic domain (e.g., Graham et al., 2013; Spadini et al., 1996) also limits our ability to constrain the timing of propagation in this area. Our observations provide initial spatiotemporal markers to constrain models of EBSB rifting and continental breakup, but ultimately more closely spaced profiles of similar quality, or even 3-D seismic data sets, will be required to determine exactly how the rift propagated.

This study highlights the similarity of EBSB evolution to that of rifted margins (e.g., Iberia-Newfoundland and Brazil-Angola margins; Brune et al., 2017; Reston et al., 1996; Tucholke & Sibuet, 2007), back-arc basins (e.g., Tyrrhenian basin (Prada et al., 2015); Aegean Sea, Japan Sea, and Yamato Basin (Jolivet et al., 1994, 1999); South China Sea (Lei & Ren, 2016); and Woodlark Basin (Taylor et al., 1995)), and rift basins elsewhere (e.g., Gulf of Suez (Gawthorpe et al., 2003) and North Sea (Cowie et al., 2005)), making the EBSB a case study for understanding the processes driving the evolution of extensional basins on a global scale.

6. Conclusions

Based on the interpretation of long-offset seismic reflection profiles, we conclude the following:

1. Overlying the EBSB rifted basement, up to 3 km of Late Cretaceous synrift deposits (S1 and S2) record an initial localized extension over the structural highs (S1), followed by rift migration toward the basin axis (S2).
2. Strain initiated along isolated high-angle normal faults (30-70° dip) over the structural highs. Some faults coalesced forming the large systems bounding the ridges (Rift Stage 1). Strain then propagated downslope toward the basin axis, forming closely spaced domino-style fault arrays characterized by lower dip angles (15°-25°). Stratigraphic contacts show that these fault arrays are younger and they sometimes affect shallower stratigraphic levels (up to S5a), recording the process of strain localization and basinward propagation (Rift Stage 2).
3. Three main unconformities are identified: (i) the *rift-onset unconformity* (U1) represents the initiation of Late Cretaceous extension, (ii) an intermediate rift unconformity (U2) records the migration of strain and the basinward younging of the synrift infill and normal faulting, and (iii) the *breakup unconformity* (U3; Upper Cretaceous-Palaeocene(?)) records breakup initiation and spreading in the SE.
4. Above the *breakup unconformity* (U3), up to 4-4.5 km of Palaeocene(?)-Eocene and Oligocene deposits (S3-S4 and S5a) show an intermediate character between synrift and postrift, recording the diachronous distribution of synkinematic and breakup processes across the EBSB. Stratigraphic and structural evidence within these units shows extension up to Oligocene time, in the NW area and along the main basin-bounding faults. In the central and SE part of the EBSB, the postrift character of these units confirms that localized breakup may have occurred before their deposition, and thus at the Late Cretaceous-Palaeocene (?) boundary, synchronous with extension in the NW.
5. The diachronous evolution of the EBSB is typical of well-studied rifted margins worldwide and provides further evidence for the need to consider continental breakup as a fully three-dimensional process that is poorly represented by a single transect.

Acknowledgments

We thank reviewers, Donna Shillington and Tiago Alves, for their constructive comments. We thank *Geology Without Limits* for making the seismic data set available to us. We are grateful to GWL for permission to show their confidential seismic sections. Parties interested in acquiring these data and corresponding data reports can contact the vendors through their websites at www.gwl-geo.com. We thank Schlumberger for providing the Petrel software that was used for seismic display, interpretation, and depth conversion. V. M. was supported by NERC Centre for Doctoral Training (CDT) in Oil and Gas. TAM was supported by a Wolfson Research Merit Award.

References

- Adamia, S. A., Gamkrelidze, I. P., Zakariadze, G. S., & Lordkipanidze, M. B. (1974). Adjara-Trialeti trough and the problem of the Black Sea origin. *Geotektonika*, 1, 78–94.
- Adamia, S. A., Chkhotua, T. G., Gavtadze, T. T., Lebanidze, Z. A., Lursmanashvili, N. D., Sadradze, N. G., et al. (2017). Tectonic setting of Georgia-eastern Black Sea: A review. *Geological Society, London, Special Publications*, 428(1), 11–40. <https://doi.org/10.1144/SP428.6>
- Alves, T. M., & Cunha, T. A. (2018). A phase of transient subsidence, sediment bypass and deposition of regressive-transgressive cycles during the breakup of Iberia and Newfoundland. *Earth and Planetary Science Letters*, 484, 168–183. <https://doi.org/10.1016/j.epsl.2017.11.054>
- Banks, C. J., Robinson, A. G., & Williams, M. P. (1997). Structure and regional tectonics of the Achara-Trialeti fold belt and the adjacent rioni and Kartli foreland basins, Republic of Georgia. In A. G. Robinson (Ed.), *Regional and petroleum geology of the Black Sea and surrounding region: AAPG Memoir*, 68, 331–346.
- Bektaş, O., & Güven, İ. H. (1995). Alaskan aphanitic type ultramafic and mafic complexes as the root zone of the Eastern Pontide Magmatic Arc (NE 48 Turkey). *Geology of the Black Sea Region*, 189–196.
- Belousov, V. V., Volvovsky, B. S., Arkhipov, I. V., Buryanova, B. V., Evsyukov, Y. D., & Goncharov, V. P. (1988). Structure and evolution of the Earth's crust and upper mantle of the Black Sea. *Bollettino di Geofisica Teorica e Applicata*, 30(117-118), 109–196.
- Bond, G. C., Kominz, M. A., & Sheridan, R. E. (1995). Continental terraces and rises. In *Tectonics of sedimentary basins*, (pp. 149–178). Oxford: Blackwell Science.
- Brune, S., Heine, C., Clift, P. D., & Pérez-Gussinyé, M. (2017). Rifted margin architecture and crustal rheology: Reviewing Iberia-Newfoundland, Central South Atlantic, and South China Sea. *Marine and Petroleum Geology*, 79, 257–281. <https://doi.org/10.1016/j.marpetgeo.2016.10.018>
- Brune, S., Heine, C., Pérez-Gussinyé, M., & Sobolev, S. V. (2014). Rift migration explains continental margin asymmetry and crustal hyper-extension. *Nature Communications*, 5, 4014. <https://doi.org/10.1038/ncomms5014>
- Buck, W. R. (1988). Flexural rotation of normal faults. *Tectonics*, 7(5), 959–973. <https://doi.org/10.1029/TC007i005p00959>
- Buckley, J. P., Bosence, D., & Elders, C. (2015). Tectonic setting and stratigraphic architecture of an Early Cretaceous lacustrine carbonate platform, Sugar Loaf High, Santos Basin, Brazil. *Geological Society, London, Special Publications*, 418, <https://doi.org/10.1144/SP418.13>
- Cloetingh, S. A. P. L., Spadini, G., Van Wees, J. D., & Beekman, F. (2003). Thermo-mechanical modelling of Black Sea Basin (de) formation. *Sedimentary Geology*, 156(1-4), 169–184. [https://doi.org/10.1016/S0037-0738\(02\)00287-7](https://doi.org/10.1016/S0037-0738(02)00287-7)
- Cohen, K. M., Harper, D. A. T., & Gibbard, P. L. (2016). International Chronostratigraphic Chart <http://stratigraphy.org/ICSchart.ChronostratChart2016-12.jpg>.
- Cowie, P. A., Gupta, S., & Dawers, N. H. (2000). Implications of fault array evolution for synrift depocenter development: Insights from a numerical fault growth model. *Basin Research*, 12, 241–261.
- Cowie, P. A., Underhill, J. R., Behn, M. D., Lin, J., & Gill, C. E. (2005). Spatio-temporal evolution of strain accumulation derived from multi-scale observations of Late Jurassic rifting in the northern North Sea: A critical test of models for lithospheric extension. *Earth and Planetary Science Letters*, 234(3-4), 401–419. <https://doi.org/10.1016/j.epsl.2005.01.039>

- Driscoll, N. W., Hogg, J. R., Christie-Blick, N., & Karner, G. D. (1995). Extensional tectonics in the Jeanne d'Arc Basin, offshore Newfoundland: Implications for the timing of break-up between Grand Banks and Iberia. *Geological Society, London, Special Publications*, 90(1), 1–28. <https://doi.org/10.1144/GSL.SP.1995.090.01.01>
- Edwards, R. A., Scott, C. L., Shillington, D. J., Minshull, T. A., Brown, P. J., & White, N. J. (2009). Wide-angle seismic data reveal sedimentary and crustal structure of the Eastern Black Sea. *The Leading Edge*, 28(9), 1056–1065. <https://doi.org/10.1190/1.3236375>
- Egan, S. S., & Meredith, D. J. (2007). A kinematic modelling approach to lithosphere deformation and basin formation: Application to the Black Sea. *Geological Society, London, Special Publications*, 282(1), 173–198. <https://doi.org/10.1144/SP282.9>
- Espurt, N., Hippolyte, J. C., Kaymakci, N., & Sangu, E. (2014). Lithospheric structural control on inversion of the southern margin of the Black Sea Basin, Central Pontides, Turkey. *Lithosphere*, 6(1), 26–34. <https://doi.org/10.1130/L316.1>
- Falvey, D. A. (1974). The development of continental margins in plate tectonic theory. *The APPEA Journal*, 14(1), 95–106. <https://doi.org/10.1071/AJ73012>
- Finetti, I., Bricchi, G., Del Ben, A., Pipan, M., & Xuan, X. (1988). Geophysical study of the Black Sea area. *Bollettino di Geofisica Teorica e Applicata*, 30(117), 197–324.
- Franke, D. (2013). Rifting, lithosphere breakup and volcanism: Comparison of magma-poor and volcanic rifted margins. *Marine and Petroleum Geology*, 43, 63–87. <https://doi.org/10.1016/j.marpetgeo.2012.11.003>
- Gawthorpe, R. L., Jackson, C. A. L., Young, M. J., Sharp, I. R., Moustafa, A. R., & Leppard, C. W. (2003). Normal fault growth, displacement localisation and the evolution of normal fault populations: The Hammam Faraun fault block, Suez rift, Egypt. *Journal of Structural Geology*, 25(6), 883–895. [https://doi.org/10.1016/S0191-8141\(02\)00088-3](https://doi.org/10.1016/S0191-8141(02)00088-3)
- Golmshtok, A. Y., Zonenshain, L. P., Terekhov, A. A., & Shainurov, R. V. (1992). Age, thermal evolution and history of the Black Sea Basin based on heat flow and multichannel reflection data. *Tectonophysics*, 210(3-4), 273–293. [https://doi.org/10.1016/0040-1951\(92\)90326-2](https://doi.org/10.1016/0040-1951(92)90326-2)
- Görür, N. (1988). Timing of opening of the Black Sea basin. *Tectonophysics*, 147(3-4), 247–262. [https://doi.org/10.1016/0040-1951\(88\)90189-8](https://doi.org/10.1016/0040-1951(88)90189-8)
- Görür, N., & Tüysüz, O. (1997). Petroleum geology of the southern continental margin of the Black Sea. In A. G. Robinson (Ed.), *Regional and petroleum geology of the Black Sea and surrounding region: AAPG Memoir* 68, 241–254.
- Görür, N., Tüysüz, O., Aykol, A., Saking, M., Yiğitbaş, E., & Akkök, R. (1993). Cretaceous red pelagic carbonates of northern Turkey: Their place in the opening history of the Black Sea. *Eclogae Geologicae Helveticae*, 86, 819–838.
- Graham, R., Kaymakci, N., & Horn, B. W. (2013). The Black Sea: Something different. *Geo Expro*, 10(5), 57–62.
- Haecker, M. A. (1992). Convergent gridding: A new approach to surface reconstruction. *Geobyte*, 7(3), 48–53.
- Hey, R., Duennebier, F. K., & Morgan, W. J. (1980). Propagating rifts on midocean ridges. *Journal of Geophysical Research*, 85(B7), 3647–3658. <https://doi.org/10.1029/JB085iB07p03647>
- Hippolyte, J. C., Müller, C., Kaymakci, N., & Sangu, E. (2010). Dating of the Black Sea Basin: New nannoplankton ages from its inverted margin in the Central Pontides (Turkey). *Geological Society, London, Special Publications*, 340(1), 113–136. <https://doi.org/10.1144/SP340.7>
- Hippolyte, J. C., Müller, C., Sangu, E., & Kaymakci, N. (2017). Stratigraphic comparisons along the Pontides (Turkey) based on new nannoplankton age determinations in the Eastern Pontides: Geodynamic implications. *Geological Society, London, Special Publications*, 428(1), 323–358. <https://doi.org/10.1144/SP428.9>
- Hippolyte, J. C., Murovskaya, A., Volfman, Y., Yegorova, T., Gintov, O., Kaymakci, N., & Sangu, E. (2018). Age and geodynamic evolution of the Black Sea Basin: Tectonic evidences of rifting in Crimea. *Marine and Petroleum Geology*, 93, 298–314. <https://doi.org/10.1016/j.marpetgeo.2018.03.009>
- Hsü, K. J., Nachev, I. K., & Vuchev, V. T. (1977). Geologic evolution of Bulgaria in light of plate tectonics. *Tectonophysics*, 40(3-4), 245–256. [https://doi.org/10.1016/0040-1951\(77\)90068-3](https://doi.org/10.1016/0040-1951(77)90068-3)
- Jolivet, L., Faccenna, C., D'Agostino, N., Fournier, M., & Worrall, D. (1999). The kinematics of back-arc basins, examples from the Tyrrhenian, Aegean and Japan Seas. *Geological Society, London, Special Publications*, 164(1), 21–53. <https://doi.org/10.1144/GSL.SP.1999.164.01.04>
- Jolivet, L., Tamaki, K., & Fournier, M. (1994). Japan Sea, opening history and mechanism: A synthesis. *Journal of Geophysical Research*, 99(B11), 22,237–22,259. <https://doi.org/10.1029/93JB03463>
- Jones, R. W., & Simmons, M. D. (1997). A review of the stratigraphy of Eastern Paratethys (Oligocene-Holocene), with particular emphasis on the Black Sea. In A. G. Robinson (Ed.), *Regional and petroleum geology of the Black Sea and surrounding region: AAPG Memoir* 68, 39–52.
- Kazmin, V. G., Schreider, A. A., & Bulychev, A. A. (2000). Early stages of evolution of the Black Sea. *Geological Society, London, Special Publications*, 173(1), 235–249. <https://doi.org/10.1144/GSL.SP.2000.173.01.12>
- Kitchka, A. A., Dovzhok, T. I., Vakarchuk, S. G., Orach, S. V., & Orach, I. A. (2014). Advancing in the Black Sea Basin Hydrocarbon Exploration-Geological Achievements vs. Industry Pitfalls. In 76th EAGE Conference and Exhibition 2014.
- Lavier, L. L., & Manatschal, G. (2006). A mechanism to thin the continental lithosphere at magma-poor margins. *Nature*, 440(7082), 324–328. <https://doi.org/10.1038/nature04608>
- Lavier, L. L., Roger Buck, W., & Poliakov, A. N. (1999). Self-consistent rolling-hinge model for the evolution of large-offset low-angle normal faults. *Geology*, 27(12), 1127–1130. [https://doi.org/10.1130/0091-7613\(1999\)027<1127:SCRHMF>2.3.CO;2](https://doi.org/10.1130/0091-7613(1999)027<1127:SCRHMF>2.3.CO;2)
- Le Pourhiet, L., Chamot-Rooke, N., Delescluse, M., May, D. A., Watremez, L., & Pubellier, M. (2018). Continental break-up of the South China Sea stalled by far-field compression. *Nature Geoscience*, 11(8), 605. <https://doi.org/10.1038/s41561-018-0178-5>
- Lei, C., Alves, T. M., Ren, J., Pang, X., Yang, L., & Liu, J. (2019). Depositional architecture and structural evolution of a region immediately inboard of the locus of continental breakup (Liwian Sub-basin, South China Sea). *Geological Society of America Bulletin*, 131(7-8), 1059–1074. <https://doi.org/10.1130/B35001.1>
- Lei, C., & Ren, J. (2016). Hyper-extended rift systems in the Xisha Trough, northwestern South China Sea: Implications for extreme crustal thinning ahead of a propagating ocean. *Marine and Petroleum Geology*, 77, 846–864. <https://doi.org/10.1016/j.marpetgeo.2016.07.022>
- Letouzey, J., Biju-Duval, B., Dorkel, A., Gonnard, R., Kristchev, K., Montadert, L., & Sungurlu, O. (1977). The Black Sea: A marginal basin; geophysical and geological data. In *International Symposium on the Structural History of the Mediterranean Basins*. Technip, Paris (pp. 363–376).
- Lundin, E. R., Redfield, T. F., Péron-Pindivic, G., & Pindell, J. (2014, January). Rifted continental margins: Geometric influence on crustal architecture and melting. In J. Pindell, B. Horn, et al. (Eds.), *Sedimentary Basins: Origin, Depositional Histories, and Petroleum Systems, 33rd Annual GCSSEPM Foundation Bob F. Perkins Conference*. Gulf Coast Section SEMP (GCSSEPM), Houston, TX, 18–53.

- Manatschal, G., Müntener, O., Lavier, L. L., Minshull, T. A., & Péron-Pinvidic, G. (2007). Observations from the Alpine Tethys and Iberia–Newfoundland margins pertinent to the interpretation of continental breakup. *Geological Society, London, Special Publications*, 282(1), 291–324. <https://doi.org/10.1144/SP282.14>
- Martin, A. K. (1984). Propagating rifts: Crustal extension during continental rifting. *Tectonics*, 3(6), 611–617. <https://doi.org/10.1029/TC003i006p00611>
- Moore, J. G. (1992). A syn-rift to post-rift transition sequence in the Main Porcupine Basin, offshore western Ireland. *Geological Society, London, Special Publications*, 62(1), 333–349. <https://doi.org/10.1144/GSL.SP.1992.062.01.26>
- Muirhead, J. D., Kattenhorn, S. A., Lee, H., Mana, S., Turrin, B. D., Fischer, T. P., et al. (2016). Evolution of upper crustal faulting assisted by magmatic volatile release during early-stage continental rift development in the East African Rift. *Geosphere*, 12(6), 1670–1700. <https://doi.org/10.1130/GES01375.1>
- Munteanu, I., Matenco, L., Dinu, C., & Cloetingh, S. A. P. L. (2011). Kinematics of back-arc inversion of the Western Black Sea Basin. *Tectonics*, 30, TC5004. <https://doi.org/10.1029/2011TC002865>
- Nagel, T. J., & Buck, W. R. (2004). Symmetric alternative to asymmetric rifting models. *Geology*, 32(11), 937–940. <https://doi.org/10.1130/G20785.1>
- Nikishin, A. M., Khotylev, A. O., Bychkov, A. Y., Kopaevich, L. F., Petrov, E. I., & Yapaskurt, V. O. (2013). Cretaceous volcanic belts and the evolution of the Black Sea Basin. *Moscow University Geology Bulletin*, 68(3), 141–154. <https://doi.org/10.3103/S0145875213030058>
- Nikishin, A. M., Korotaev, M. V., Ershov, A. V., & Brunet, M. F. (2003). The Black Sea basin: Tectonic history and Neogene–Quaternary rapid subsidence modelling. *Sedimentary Geology*, 156(1–4), 149–168. [https://doi.org/10.1016/S0037-0738\(02\)00286-5](https://doi.org/10.1016/S0037-0738(02)00286-5)
- Nikishin, A. M., Okay, A., Tüysüz, O., Demirel, A., Wannier, M., Amelin, N., & Petrov, E. (2015b). The Black Sea basins structure and history: New model based on new deep penetration regional seismic data. Part 2: Tectonic history and paleogeography. *Marine and Petroleum Geology*, 59, 656–670. <https://doi.org/10.1016/j.marpetgeo.2014.08.018>
- Nikishin, A. M., Okay, A. I., Tüysüz, O., Demirel, A., Amelin, N., & Petrov, E. (2015a). The Black Sea basins structure and history: New model based on new deep penetration regional seismic data. Part 1: Basins structure and fill. *Marine and Petroleum Geology*, 59, 638–655. <https://doi.org/10.1016/j.marpetgeo.2014.08.017>
- Nikishin, A. M., Wannier, M., Alekseev, A. S., Almendinger, O. A., Fokin, P. A., Gabdullin, R. R., et al. (2015). Mesozoic to recent geological history of southern Crimea and the Eastern Black Sea region. *Geological Society, London, Special Publications*, 428(1), 241–264. <https://doi.org/10.1144/SP428.1>
- Nikishin, A. M., Ziegler, P. A., Bolotov, S. N., & Fokin, P. A. (2011). Late Palaeozoic to Cenozoic evolution of the Black Sea–Southern Eastern Europe region: A view from the Russian platform. *Turkish Journal of Earth Sciences*, 20, 571–634. <https://doi.org/10.3906/yer-1005-22>
- Nirrengarten, M., Manatschal, G., Tugend, J., Kuszniir, N., & Sauter, D. (2018). Kinematic evolution of the southern North Atlantic: Implications for the formation of hyperextended rift systems. *Tectonics*, 37, 89–118. <https://doi.org/10.1002/2017TC004495>
- Nixon, C. W., McNeill, L. C., Bull, J. M., Bell, R. E., Gawthorpe, R. L., Henstock, T. J., et al. (2016). Rapid spatiotemporal variations in rift structure during development of the Corinth Rift, central Greece. *Tectonics*, 35, 1225–1248. <https://doi.org/10.1002/2015TC004026>
- Okay, A. I., Celal Sengor, A. M., & Görür, N. (1994). Kinematic history of the opening of the Black Sea and its effect on the surrounding regions. *Geology*, 22(3), 267–270. [https://doi.org/10.1130/0091-7613\(1994\)022<0267:KHOTOO>2.3.CO;2](https://doi.org/10.1130/0091-7613(1994)022<0267:KHOTOO>2.3.CO;2)
- Okay, A. I., & Şahintürk, O. (1997). Geology of the Eastern Pontides. In A. G. Robinson (Ed.), *Regional and petroleum geology of the Black Sea and surrounding region: AAPG Memoir 68*, 291–311.
- Okay, A. I., Sunal, G., Sherlock, S., Altiner, D., Tüysüz, O., Kylander-Clark, A. R., & Aygül, M. (2013). Early Cretaceous sedimentation and orogeny on the active margin of Eurasia: Southern Central Pontides, Turkey. *Tectonics*, 32, 1247–1271. <https://doi.org/10.1002/tect.20077>
- Okay, A. I., & Tüysüz, O. (1999). Tethyan sutures of northern Turkey. *Geological Society, London, Special Publications*, 156(1), 475–515. <https://doi.org/10.1144/GSL.SP.1999.156.01.22>
- Olsen, P. E. (1997). Stratigraphic record of the early Mesozoic breakup of Pangea in the Laurasia–Gondwana rift system. *Annual Review of Earth and Planetary Sciences*, 25(1), 337–401. <https://doi.org/10.1146/annurev.earth.25.1.337>
- Péron-Pinvidic, G., & Manatschal, G. (2009). The final rifting evolution at deep magma-poor passive margins from Iberia–Newfoundland: A new point of view. *International Journal of Earth Sciences*, 98(7), 1581–1597. <https://doi.org/10.1007/s00531-008-0337-9>
- Péron-Pinvidic, G., Manatschal, G., Masini, E., Sutra, E., Flament, J. M., Hauptert, I., & Unternehr, P. (2017). Unravelling the along-strike variability of the Angola–Gabon rifted margin: A mapping approach. *Geological Society, London, Special Publications*, 438(1), 49–76. <https://doi.org/10.1144/SP438.1>
- Péron-Pinvidic, G., Manatschal, G., Minshull, T. A., & Sawyer, D. S. (2007). Tectonosedimentary evolution of the deep Iberia–Newfoundland margins: Evidence for a complex breakup history. *Tectonics*, 26, TC2011. <https://doi.org/10.1029/2006TC001970>
- Prada, M., Sallarès, V., Ranero, C. R., Vendrell, M. G., Grevemeyer, I., Zitellini, N., & de Franco, R. (2015). The complex 3-D transition from continental crust to backarc magmatism and exhumed mantle in the Central Tyrrhenian basin. *Geophysical Journal International*, 203(1), 63–78. <https://doi.org/10.1093/gji/ggv271>
- Ranero, C. R., & Pérez-Gussinyé, M. (2010). Sequential faulting explains the asymmetry and extension discrepancy of conjugate margins. *Nature*, 468(7321), 294. <https://doi.org/10.1038/nature09520>
- Rangin, C., Bader, A. G., Pascal, G., Ecevitoglu, B., & Görür, N. (2002). Deep structure of the Mid Black Sea High (offshore Turkey) imaged by multi-channel seismic survey (BLACKSIS cruise) 1, 2. *Marine Geology*, 182(3–4), 265–278. [https://doi.org/10.1016/S0025-3227\(01\)00236-5](https://doi.org/10.1016/S0025-3227(01)00236-5)
- Reston, T. J. (2005). Polyphase faulting during the development of the west Galicia rifted margin. *Earth and Planetary Science Letters*, 237(3–4), 561–576. <https://doi.org/10.1016/j.epsl.2005.06.019>
- Reston, T. J., Krawczyk, C. M., & Klaeschen, D. (1996). The S reflector west of Galicia (Spain): Evidence from prestack depth migration for detachment faulting during continental breakup. *Journal of Geophysical Research*, 101(B4), 8075–8091. <https://doi.org/10.1029/95JB03466>
- Robinson, A., Spadini, G., Cloetingh, S., & Rudat, J. (1995). Stratigraphic evolution of the Black Sea: Inferences from basin modelling. *Marine and Petroleum Geology*, 12(8), 821–835. [https://doi.org/10.1016/0264-8172\(95\)98850-5](https://doi.org/10.1016/0264-8172(95)98850-5)
- Robinson, A. G., Banks, C. J., Rutherford, M. M., & Hirst, J. P. P. (1995). Stratigraphic and structural development of the Eastern Pontides, Turkey. *Journal of the Geological Society*, 152(5), 861–872. <https://doi.org/10.1144/gsjgs.152.5.0861>
- Robinson, A. G., Rudat, J. H., Banks, C. J., & Wiles, R. L. F. (1996). Petroleum geology of the Black Sea. *Marine and Petroleum Geology*, 13(2), 195–223. [https://doi.org/10.1016/0264-8172\(95\)00042-9](https://doi.org/10.1016/0264-8172(95)00042-9)

- Ross, D. A. (1978). Summary of results of Black Sea drilling. Initial Reports of the Deep Sea Drilling Project, 42(Part 2).
- Rudat, J. H., & MacGregor, D. S. (1993). Unconventional exploration techniques in a high cost deep water basin: A case study from the Black Sea. Society of Exploration Geophysicists. In Abstracts with Programs. <https://doi.org/10.1190/1.1822382>
- Saintot, A., Brunet, M. F., Yakovlev, F., Sébrier, M., Stephenson, R., Ershov, A., et al. (2006). The Mesozoic-Cenozoic tectonic evolution of the Greater Caucasus. *Geological Society, London, Memoirs*, 32(1), 277–289. <https://doi.org/10.1144/GSL.MEM.2006.032.01.16>
- Scott, C. L., Shillington, D. J., Minshull, T. A., Edwards, R. A., Brown, P. J., & White, N. J. (2009). Wide-angle seismic data reveal extensive overpressures in the Eastern Black Sea Basin. *Geophysical Journal International*, 178(2), 1145–1163. <https://doi.org/10.1111/j.1365-246X.2009.04215.x>
- Sheremet, Y., Sosson, M., Ratzov, G., Sydorenko, G., Voitsitskiy, Z., Yegorova, T., et al. (2016). An offshore-onland transect across the north-eastern Black Sea basin (Crimean margin): Evidence of Paleocene to Pliocene two-stage compression. *Tectonophysics*, 688, 84–100. <https://doi.org/10.1016/j.tecto.2016.09.015>
- Shillington, D. J., Minshull, T. A., Edwards, R. A., & White, N. (2017). Crustal structure of the Mid Black Sea High from wide-angle seismic data. *Geological Society, London, Special Publications*, 464, SP464–SP466. <https://doi.org/10.1144/SP464.6>
- Shillington, D. J., Scott, C. L., Minshull, T. A., Edwards, R. A., Brown, P. J., & White, N. (2009). Abrupt transition from magma-starved to magma-rich rifting in the eastern Black Sea. *Geology*, 37(1), 7–10. <https://doi.org/10.1130/G25302A.1>
- Shillington, D. J., White, N., Minshull, T. A., Edwards, G. R., Jones, S. M., Edwards, R. A., & Scott, C. L. (2008). Cenozoic evolution of the eastern Black Sea: A test of depth-dependent stretching models. *Earth and Planetary Science Letters*, 265(3-4), 360–378. <https://doi.org/10.1016/j.epsl.2007.10.033>
- Shreider, A. A. (2005). Opening of the deep-water basin of the Black Sea. *Oceanology*, 45(4), 560–571.
- Shreider, A. A., Kazmin, V. G., & Lygin, V. S. (1997). Magnetic anomalies and age of the Black Sea Deep Basins. *Geotectonics*, 31(1), 54–64.
- Slotnick, M. M. (1936). On seismic computations, with applications. *J. Geophysics*, 1(1), 9–22. <https://doi.org/10.1190/1.1437084>
- Soares, D. M., Alves, T. M., & Terrinha, P. (2012). The breakup sequence and associated lithospheric breakup surface: Their significance in the context of rifted continental margins (West Iberia and Newfoundland margins, North Atlantic). *Earth and Planetary Science Letters*, 355, 311–326. <https://doi.org/10.1016/j.epsl.2012.08.036>
- Spadini, G., Robinson, A., & Cloetingh, S. (1996). Western versus Eastern Black Sea tectonic evolution: Pre-rift lithospheric controls on basin formation. *Tectonophysics*, 266(1-4), 139–154. [https://doi.org/10.1016/S0040-1951\(96\)00187-4](https://doi.org/10.1016/S0040-1951(96)00187-4)
- Stephenson, R., & Schellart, W. P. (2010). The Black Sea back-arc basin: Insights to its origin from geodynamic models of modern analogues. *Geological Society, London, Special Publications*, 340(1), 11–21. <https://doi.org/10.1144/SP340.2>
- Stovba, S., Khriachtchevskaia, O., & Popadyuk, I. (2009). Hydrocarbon-bearing areas in the eastern part of the Ukrainian Black Sea. *The Leading Edge*, 28(9), 1042–1045. <https://doi.org/10.1190/1.3236373>
- Sutra, E., Manatschal, G., Mohn, G., & Unternehr, P. (2013). Quantification and restoration of extensional deformation along the Western Iberia and Newfoundland rifted margins. *Geochemistry, Geophysics, Geosystems*, 14, 2575–2597. <https://doi.org/10.1002/ggge.20135>
- Sydorenko, G., Stephenson, R., Yegorova, T., Starostenko, V., Tolkunov, A., Janik, T., et al. (2017). Geological structure of the northern part of the Eastern Black Sea from regional seismic reflection data including the DOBRE-2 CDP profile. *Geological Society, London, Special Publications*, 428(1), 307–321. <https://doi.org/10.1144/SP428.15>
- Tari, G. (2015). Is the Black Sea really a back-arc basin? In: Transactions of the GCSEPM Foundation Perkins–Rosen 34th Annual Research Conference 'Petroleum Systems in Rift Basins', 510–520.
- Tari, G., Vakhania, D., Tatishvili, G., Mikeladze, V., Gogritchiani, K., Vacharadze, S., et al. (2018). Stratigraphy, structure and petroleum exploration play types of the Rioni Basin, Georgia. *Geological Society, London, Special Publications*, 464(1), 403–438. <https://doi.org/10.1144/SP464.14>
- Tari, G. C., & Simmons, M. D. (2018). History of deepwater exploration in the Black Sea and an overview of deepwater petroleum play types. *Geological Society, London, Special Publications*, 464(1), 439–475. <https://doi.org/10.1144/SP464.16>
- Taylor, B., Goodliffe, A., Martinez, F., & Hey, R. (1995). Continental rifting and initial sea-floor spreading in the Woodlark Basin. *Nature*, 374(6522), 534–537. <https://doi.org/10.1038/374534a0>
- Tucholke, B. E., & Sibuet, J. C. (2007). Leg 210 synthesis: Tectonic, magmatic, and sedimentary evolution of the Newfoundland-Iberia rift. In *Proceedings of the Ocean Drilling Program. scientific results*, (Vol. 210, pp. 1–56). College Station, TX: Ocean Drilling Program.
- Tugend, J., Manatschal, G., Kusznir, N. J., & Masini, E. (2015). Characterizing and identifying structural domains at rifted continental margins: Application to the Bay of Biscay margins and its Western Pyrenean fossil remnants. *Geological Society, London, Special Publications*, 413(1), 171–203. <https://doi.org/10.1144/SP413.3>
- Tugolesov, D. A., Gorshkov, A. S., Meysner, L. B., Soloviov, V. V., Khakhalev, E. M., Akilova, Y. V., et al. (1985). Tectonics of the Mesozoic sediments of the Black Sea basin. Nedra, Moscow, 215.
- Tüysüz, O. (1999). Geology of the Cretaceous sedimentary basins of the Western Pontides. *Geological Journal*, 34(1-2), 75–93. [https://doi.org/10.1002/\(SICI\)1099-1034\(199901/06\)34:1/2<75::AID-GJ815>3.0.CO;2-S](https://doi.org/10.1002/(SICI)1099-1034(199901/06)34:1/2<75::AID-GJ815>3.0.CO;2-S)
- Tüysüz, O., Yılmaz, İ. Ö., Svabnicka, L., & Kirici, S. (2012). The Unaz formation: A key unit in the Western Black Sea region, N Turkey. *Turkish Journal of Earth Sciences*, 21(6), 1009–1028. <https://doi.org/10.3906/yer-1006-30>
- Verzhbitsky, E., Kuzin, I., & Lobkovsky, L. (2002). Age and thickness of the lithosphere within the Western and Eastern basins of the Black Sea according to geophysical data. *Turkish Journal of Earth Sciences*, 11(3), 231–242.
- Vincent, S. J., Braham, W., Lavrishchev, V. A., Maynard, J. R., & Harland, M. (2016). The formation and inversion of the western Greater Caucasus Basin and the uplift of the western Greater Caucasus: Implications for the wider Black Sea region. *Tectonics*, 35, 2948–2962. <https://doi.org/10.1002/2016TC004204>
- Vink, G. E. (1982). Continental rifting and the implications for plate tectonic reconstructions. *Journal of Geophysical Research*, 87(B13), 10,677–10,688. <https://doi.org/10.1029/JB087iB13p10677>
- Westphal, M., Bazhenov, M. L., Lauer, J. P., Pechersky, D. M., & Sibuet, J. C. (1986). Paleomagnetic implications on the evolution of the Tethys belt from the Atlantic Ocean to the Pamirs since the Triassic. *Tectonophysics*, 123(1-4), 37–82. [https://doi.org/10.1016/0040-1951\(86\)90193-9](https://doi.org/10.1016/0040-1951(86)90193-9)
- Williams, G. D. (1993). Tectonics and seismic sequence stratigraphy: An introduction. *Geological Society, London, Special Publications*, 71(1), 1–13. <https://doi.org/10.1144/GSL.SP.1993.071.01.01>
- Withjack, M. O., Schlische, R. W., & Olsen, P. E. (1998). Diachronous rifting, drifting, and inversion on the passive margin of central eastern North America: An analog for other passive margins. *AAPG bulletin*, 82(5), 817–835.
- Withjack, M. O., Schlische, R. W., & Olsen, P. E. (2002). Rift-basin structure and its influence on sedimentary systems. *SEPM Special Publication*, 73, 57–81.

- Yegorova, T., Baranova, E., & Omelchenko, V. (2010). The crustal structure of the Black Sea from the reinterpretation of deep seismic sounding data acquired in the 1960. *Geological Society, London, Special Publications*, 340(1), 43–56. <https://doi.org/10.1144/SP340.4>
- Yilmaz, A., Adamia, S., Chabukiani, A., Chkhotua, T., ErdoĖan, K., Tuzcu, S., & KarabiyikoĖlu, M. (2000). Structural correlation of the southern Transcaucasus (Georgia)-eastern Pontides (Turkey). *Geological Society, London, Special Publications*, 173(1), 171–182. <https://doi.org/10.1144/GSL.SP.2000.173.01.08>
- Zhou, D., Ru, K., & Chen, H. Z. (1995). Kinematics of Cenozoic extension on the South China Sea continental margin and its implications for the tectonic evolution of the region. *Tectonophysics*, 251(1-4), 161–177. [https://doi.org/10.1016/0040-1951\(95\)00018-6](https://doi.org/10.1016/0040-1951(95)00018-6)
- Zonenshain, L. P., & Le Pichon, X. (1986). Deep basins of the Black Sea and Caspian Sea as remnants of Mesozoic back-arc basins. *Tectonophysics*, 123(1-4), 181–211. [https://doi.org/10.1016/0040-1951\(86\)90197-6](https://doi.org/10.1016/0040-1951(86)90197-6)